Modern sand provenance and transport across the western Gulf of Mexico margin

Timothy F. Lawton[1,†], Edgar Juárez-Arriaga[2], Daniel F. Stockli[3], and Andrea Fildani[4]

[1]*Bureau of Economic Geology, Jackson School of Geosciences, The University of Texas at Austin, Austin, Texas 78758, USA*
[2]*Instituto de Geología, Universidad Nacional Autónoma de México, Ciudad Universitaria, Coyoacán, 04510, Ciudad de México, México*
[3]*Department of Geological Sciences, Jackson School of Geosciences, The University of Texas at Austin, Austin, Texas 78712, USA*
[4]*The Deep Time Institute, 23 Railroad Avenue #804, Danville, California 94526, USA*

ABSTRACT

Petrographic and detrital zircon U-Pb analysis of modern beach sands and river sands from major catchments in northeastern Mexico draining to the Gulf of Mexico provides evidence for a minimum of 650 km of littoral sand transport southward from the mouth of the Rio Grande at the Mexico-U.S. border to the central part of the state of Veracruz, Mexico. Principal tracers of Rio Grande sand include: (1) quartzose composition that contrasts with lithic compositions of sand in eastern Mexico rivers and (2) detrital zircon ages with Mesoproterozoic modes at 1.8–1.5 Ga and 1.4 Ga, age groups that are typical of basement and derivative sediment of the SW United States but are uncommon to rare in Mexican river catchments. In contrast, abundant Miocene and younger grains in beach sands of Veracruz indicate primary sediment derivation from active and recently active volcanoes in the Trans-Mexican volcanic belt in central Mexico. A proportional decrease in sand of Rocky Mountain provenance with distance southward along the coast from the mouth of the Rio Grande and absence of Miocene and younger zircon grains in beaches north of rivers draining the Trans-Mexican volcanic belt indicate net littoral sand transport southward along the eastern coast of Mexico, demonstrating that wintertime shoreline-parallel surface currents rather than north-directed summertime currents dominate sediment transfer. Sand samples of Tamaulipas beaches in northeastern Mexico commonly have equal or higher proportions of U.S.-derived Mesoproterozoic zircon grains than are present in

river bar sand of the lower Rio Grande and the Rio Grande delta, and thus require that littoral processes rework and incorporate coastal dune and beach sands of northeastern Mexico that are enriched in predam Rio Grande sediment. Implied coastal erosion may be related to Holocene transgression or interruption of sediment supply to the coastal sediment transport system by dams in the Rio Grande drainage basin. Such coastal erosion is impacting long-term shoreline stability and viability of the littoral environment.

INTRODUCTION

The composition and detrital geochronology of modern sand provide critical insights into recent sediment dispersal pathways and transport processes (Garzanti et al., 2012, 2017) and potential anthropogenic impacts on sediment budget along sediment transport routes (Thomson et al., 2022). Modern sand composition can establish actualistic benchmarks for sources of ancient detritus and provide important lines of evidence for modern sediment dispersal and transport processes that have become fundamental to improved understanding of the highly sensitive transition between sea and land (e.g., Van Andel and Poole, 1960; Garzanti et al., 2012, 2017; van de Kamp, 2018). The sea-land interface is critical to human economies and coastal ecosystems; therefore, coastal integrity in the context of predicted long-term sea-level rise demands improved understanding of sediment budgets of detritus reaching the sensitive region represented by beaches and adjacent marine shelves. U-Pb detrital zircon provenance analysis is an effective tool for tracing sediment transport at the sea-land interface, estimating sediment budgets of beaches and contributive rivers, and evaluating potential anthropogenic impacts on the sediment budget (e.g., Moore et al., 2021; Giles et al., 2023).

Extensive thermochronologic data sets, including apatite and zircon fission-track analyses and (U-Th)/He zircon analyses, indicate that northeastern and eastern Mexico has experienced widespread regional uplift and exhumation from at least 45 Ma (middle Eocene) to the present (Gray et al., 2001, 2020) and therefore predict that the area is an important source for modern sediment. The implied resultant erosion and transport of large volumes of sediment raise important questions concerning avenues of sediment dispersal and ultimate detrital sinks, particularly in the deep Gulf of Mexico, during the Cenozoic (e.g., Hessler et al., 2018; Hudec et al., 2020). Northern and central Mexico also has hosted Cenozoic and modern subduction-related magmatism (Ferrari et al., 2002, 2007, 2012; Bryan et al., 2008), and its rivers and beaches thus contain an understudied category of modern sands derived from active volcanic terranes. For the above reasons, insight into the composition of modern sediment has significant application to understanding ancient Gulf of Mexico sediment dispersal systems (e.g., Ramos-Vázquez and Armstrong-Altrin, 2021) as well as polarity and mechanisms of ongoing sand transport in the Gulf of Mexico basin.

To establish the composition of sediment at the sea-land interface along the western Gulf of Mexico and to provide a baseline for the nature of fluvial sediment derived from Mexican source rocks, we present a data set of petrographic modal compositions and detrital zircon U-Pb ages for 26 samples of river sand from catchments that drain to the Gulf of Mexico basin, seven samples of beach sand from the northwestern Gulf of Mexico, and one sample of coastal dune sand. The data set provides preliminary insight into the relative importance of primary fluvial and reworked littoral inputs into coastal sediment budgets for this part of Mexico, where the coastline is affected by seasonally opposed surface currents that are north-directed from

Timothy F. Lawton ⃝ https://orcid.org/0000-0001-6828-5047
†tim.lawton@beg.utexas.edu

Figure 1. Generalized geologic map of the southwestern United States and northern Mexico, showing rivers of this study draining to the Gulf of Mexico and principal rivers that drain to the Pacific Ocean. Bold text indicates states of Mexico and the United States mentioned in text. Orange circles represent communities mentioned in text. Thick barbed lines represent the thrust front of the Sierra Madre (SM) Oriental north of the Trans-Mexican volcanic belt and approximate width of the Sierra Zongolica thrust belt south of the Trans-Mexican volcanic belt (for details, see Fitz-Díaz et al., 2018). Mesa Central is the internally drained, high-standing topography west and south of the frontal part of the Sierra Madre Oriental. The basin and range province lying northwest of the Mesa Central extends to southern New Mexico. It is largely internally drained, traversed only by the Rio Grande and Río Conchos. HyU—Huayacocotla uplift; HzU—Huizachal uplift; JMVF—Jemez Mountains volcanic field; TLAX—Tlaxcala. Inset rectangle indicates area of Figure 2.

tain basement ages in beach sand. Greater proportions of Mesoproterozoic ages in beach sand of central Tamaulipas relative to Rio Grande fluvial sand also imply erosion and recycling of older coastal sediment in northeastern Mexico.

METHODS

Fluvial samples were collected from rivers draining to the Gulf of Mexico from the Rio Grande on the international border to the Río La Antigua in central Veracruz directly south of the Trans-Mexican volcanic belt (Figs. 1 and 2; Table 1). Approximately 5 kg aliquots of sediment were collected from surface sediment and air dried if necessary. Fluvial sands were collected in May, during the latter part of the dry season, when rivers were at their minimum discharge, and high-water sand bars were locally exposed. Samples were collected from shallow pits excavated in low-water bars or dredge piles where sand was abundant, or by carefully collecting sand from small dunes and matrix of gravel bars in the upstream reaches of rivers, which are commonly sand-poor due to dams higher in the catchments.

Beach samples were collected from central Tamaulipas at La Pesca, Tamaulipas, to Playa Chachalacas in central Veracruz, also just south of the Trans-Mexican volcanic belt (Fig. 2; Table 1). Due to logistical exigencies, sand samples of most beaches were collected

April through August and south-directed from September through March (Zavala-Hidalgo et al., 2003). Although most samples are biased by fundamental anthropogenic modifications to both fluvial and coastal sediment transport, such as hydroelectric dams, large-scale sand harvesting, and jetties, the data set supports the hypothesis that sand was and is not transported from coastal Veracruz in Mexico to the Rio Grande delta (e.g., Moore et al., 2021) along the western Gulf of Mexico littoral zone. Moreover, detrital zircon U-Pb data reveal long-distance net southward coastal sediment transport of at least 650 km on the basis of persistent Rocky Moun-

Figure 2. Generalized geologic map of northeastern Mexico with river networks and locations of samples described in text. Rivers draining to the Pacific Ocean are not indicated. Geologic units are as in Figure 1. Kss—siliciclastic strata of Difunta Group in Sierra Madre foreland; LM—La Malinche; LT—Los Tuxtlas volcanic field; PO—Pico de Orizaba; SMOVF—Sierra Madre Occidental volcanic field. Orange circles represent communities mentioned in text. Red triangles in Trans-Mexican volcanic belt represent Quaternary stratovolcanoes. Sample localities: red circles—beach samples; light blue circles—river samples; white circle—dune sample. Sample numbers indicated by numerals only are 17EMX samples (e.g., 04 is 17EMX04); other samples are written out in full. Sample 17EMX18 was collected on the Río Atlapexco. Samples GOM-56 and RG are Rio Grande sand samples of Blum et al. (2017) and Fan et al. (2019).

in May 2017, during early development of north-directed surface currents along the coast, whereas samples at Playa Chachalacas in Veracruz (17SMX38) and La Pesca in Tamaulipas (17NEMX07) were collected in February 2017 and January 2018, late in the period of south-directed surface currents. Most sample pits revealed the presence of heavy mineral laminae; both heavy mineral laminae and light mineral layers were collected in an attempt to avoid bias to the bulk sediment composition. We also col-

lected a sand sample for petrography at a coastal dune field in central Veracruz. We include in the detrital zircon data set two composites of published beach samples from southern Tamaulipas collected in October 2017 (Ramos-Vázquez and Armstrong-Altrin, 2021).

For sand petrography, unsieved sand was mounted in epoxy, cut into billets, and polished prior to mounting on glass slides for thin sections and then ground to 30 μm thickness and stained with sodium cobaltinitrite to facilitate the

identification of potassium feldspar. Four-hundred grains were counted using the Gazzi-Dickinson technique to minimize the effect of grain size on composition (e.g., Ingersoll et al., 1984) and to achieve a 2σ confidence level of ±5% or less depending upon grain proportion in the sample (Van der Plas and Tobi, 1965). Resulting point counts were plotted on standard ternary diagrams, including total quartz-feldspar-lithic (QtFL), monocrystalline quartz–feldspar–total lithic (QmFLt), metamorphic lithic–volcanic

TABLE 1. SAMPLE LOCATIONS AND MAXIMUM DEPOSITIONAL AGES (MDAs) OF SANDS FROM EASTERN MEXICO RIVERS AND BEACHES

Sample	River	State	Latitude (°N)	Longitude (°W)	MDA* (Ma) (n)	MSWD†	YSG§ (Ma)	Notes
Lower Rio Grande catchment								
RG	Rio Grande	Texas, USA	27.540934	99.512139			1.3 ± 0.1	Fan et al. (2019), approx. location
GOM-56	Rio Grande	Texas, USA	27.44168	99.49457			21.7 ± 1.7	Blum et al. (2017)
17RG01	Rio Grande	Texas, USA	25.837792	97.404053	13.7 ± 5.5 (2)	5.8	12.99 ± 0.69	
17RG02	Rio Grande	Texas, USA	25.837458	97.395789	21.61 ± 0.52 (2)	0.54	11.09 ± 0.72	
17NEMX01	Río San Juan	Nuevo León, Mexico	25.521050	100.010467	75.05 ± 0.69 (2)	0.089	70.4 ± 1.2	
17NEMX04	Río Ramos	Nuevo León, Mexico	25.260800	99.998517	84.41 ± 0.53 (4)	0.14	84.2 ± 1.0	
17NEMX02	Río Pilón	Nuevo León, Mexico	25.172450	99.865733	80.19 ± 0.36 (7)	0.73	77.1 ± 1.3	
Rivers draining to northern Gulf of Mexico								
17NEMX05	Río Pablillo	Nuevo León, Mexico	24.902683	99.468467	69.84 ± 0.32 (4)	2.3	32.8 ± 1.0	Río San Fernando on GoogleEarth
17NEMX06	Río Purificación	Tamaulipas, Mexico	24.079117	99.122550	32.3 ± 7.6 (2)	2.4	31.7 ± 1.1	Gravel bar (Río Soto La Marina catchment)
Río Pánuco catchment								
17EMX19	Río Calabozo	Veracruz, Mexico	21.285514	98.375442	58.6 ± 8.7 (2)	4.5	0.222 ± 0.044	
17EMX16	Río Garcés	Hidalgo, Mexico	20.938606	98.268614	62 ± 12 (2)	5.5	0.306 ± 0.042	
17EMX18	Río Atlapexco	Hidalgo, Mexico	21.015618	98.339199	241.2 ± 2.7 (7)	2.7	2.18 ± 0.26	
17EMX29	Río Tamuin	San Luis Potosí, Mexico	22.001199	98.772221	29.76 ± 0.16 (21)	0.74	28.3 ± 1.5	Dredged channel sand
17EMX21	Río Amajac	San Luis Potosí, Mexico	21.200111	98.784922	0.38 ± 0.53 (2)	1.8	0.030 ± 0.022	
17EMX20	Río Amajac	San Luis Potosí, Mexico	21.226768	98.754809	2.2 ± 1.6 (2)	0.15	0.192 ± 0.046	
17EMX22	Río Moctezuma	San Luis Potosí, Mexico	21.257658	98.791804	2.90 ± 0.58 (3)	2.5	0.079 ± 0.029	
17EMX23	Río Moctezuma	San Luis Potosí, Mexico	21.372050	98.766017	6.95 ± 0.24 (6)	1.8	0.21 ± 0.12	Predam point bar
17EMX25	Río Moctezuma	San Luis Potosí, Mexico	21.593367	98.656500	0.231 ± 0.057	0.33	0.172 ± 0.063	
17EMX26	Río Moctezuma	Veracruz, Mexico	21.777946	98.451624	0.12 ± 0.11 (3)	2.3	0.010 ± 0.016	High-water attached bar
Veracruz rivers								
17EMX15	Río Vinazco	Veracruz, Mexico	20.952353	97.795757	4.76 ± 0.54 (2)	1.5	4.33 ± 0.22	
17EMX12	Río Pantepec	Veracruz, Mexico	20.895327	97.788768	4.68 ± 0.13 (6)	0.71	4.25 ± 0.22	
17EMX14	Río Pantepec	Veracruz, Mexico	20.928840	97.679669	4.146 ± 0.093 (3)	0.26	4.12 ± 0.15	
17EMX11	Río Pantepec	Veracruz, Mexico	20.917167	97.565733	4.277 ± 0.074 (3)	0.17	2.73 ± 0.20	
17EMX08	Río Cazones	Veracruz, Mexico	20.490713	97.563500	1.39 ± 0.15 (2)	0.2	1.36 ± 0.20	
17EMX06	Río Tecolutla	Veracruz, Mexico	20.399978	97.232732	0.101 ± 0.019 (9)	0.53	0.065 ± 0.019	
17EMX05	Río Tecolutla	Veracruz, Mexico	20.454636	97.194776	0.155 ± 0.027 (11)	1.5	−0.07 ± 0.12	Next youngest grain = 0.093 ± 0.042 Ma
17EMX03	Río Nautla	Veracruz, Mexico	20.150296	96.899209	3.69 ± 0.28 (4)	1.3	2.04 ± 0.32	
17SMX37	Río La Antigua	Veracruz, Mexico	19.347766	96.357341	0.109 ± 0.026 (13)	1.2	0.03 ± 0.11	
Gulf of Mexico beaches								
17NEMX07	Playa La Pesca	Tamaulipas, Mexico	23.777698	97.734955	26.1 ± 1.0 (3)	1.6	3.83 ± 0.16	
PBT (N = 2)#	Playa Barra del Tordo	Tamaulipas, Mexico	23.125217	97.764733	1.200 ± 0.093 (2)	0	1.2 ± 0.1	Ramos-Vázquez and Armstrong-Altrin (2021)
PT (N = 2)#	Playa Tesoro	Tamaulipas, Mexico	22.495108	97.852219	26.6 ± 1.1 (4)	1.5	23.3 ± 0.8	Ramos-Vázquez and Armstrong-Altrin (2021)
17EMX27	Playa Miramar	Tamaulipas, Mexico	22.270380	97.788789	29.28 ± 0.50 (5)	0.95	3.32 ± 0.36	0.8 km N of mouth of Río Pánuco
17EMX28	Playa Hermosa	Veracruz, Mexico	22.194675	97.790728	3.1 ± 1.0 (2)	1.11	0.125 ± 0.040	7 km S of mouth of Río Pánuco
17EMX09	Playa Tuxpan	Veracruz, Mexico	20.983431	97.314301	30.44 ± 0.16 (18)	1.04	0.160 ± 0.018	
17EMX04	Playa Tecolutla	Veracruz, Mexico	20.482224	97.005768	1.1 ± 1.1 (2)	2.6	1.06 ± 0.12	
17EMX02	Playa Nautla	Veracruz, Mexico	20.213164	96.759845	0.35 ± 0.57 (2)	2.8	0.328 ± 0.061	
17EMX01	Dunes at Emilio Carranza	Veracruz, Mexico	19.912162	96.522957				Petrographic sample only
17EMX01B	Beach at Santa Ana	Veracruz, Mexico	19.893083	96.496500				Petrographic sample only
17SMX38	Playa Chachalacas	Veracruz, Mexico	19.419351	96.320440	1.183 ± 0.074 (5)	1.11	1.1 ± 0.27	At mouth of Río Actopan

*Weighted mean maximum depositional age (number of grains used in calculation).
†Mean square of weighted deviates (MSWD).
§Youngest single grain (YSG) age.
#N = number of samples.

lithic–sedimentary lithic (LmLvLs), and monocrystalline quartz–potassium feldspar–plagioclase (QmPK) ternary plots (e.g., Ingersoll and Suczek, 1979; Dickinson et al., 1983; Dickinson, 1985). Because many samples contained abundant volcanic lithic fragments (Lv), sands with greater than 20% total Lv were plotted on felsitic volcanic–microlitic volcanic–lathwork volcanic (LvfLvmiLvl) and vitric volcanic–microlitic volcanic–lathwork volcanic (LvvLvmiLvl) ternary diagrams that display only the Lv grain fraction (Marsaglia, 1991; Marsaglia

and Ingersoll, 1992; Critelli and Ingersoll, 1995) to establish additional detail regarding volcanic sediment sources.

Detrital-zircon U-Pb geochronology analyses were conducted at the UTChron Laboratory at the University of Texas at Austin. Individual zircon grains were separated from bulk sand samples using traditional heavy mineral separation methods, which included disc-mill grinding, Gemini water table concentration, dense liquid separation, and Frantz magnetic susceptibility separation. Zircon grains were sprinkle-mounted onto double-sided tape on 2.5-cm-diameter acrylic discs and analyzed by depth-profiling laser ablation–inductively coupled plasma–mass spectrometry (LA-ICP-MS) following the procedures of Marsh and Stockli (2015) using a laser spot 30 μm in diameter, an energy density of ~1.98 J/cm^2, and a pulse rate of 10 Hz to ablate to a depth of ~15 μm. Ablation rates were calibrated using a Bruker Contour GT-K1 optical profilometer, with 30 s ablation duration translating into ~15 μm depth or an average ablation rate of 0.5 μm/s. Continuous depth-profile analysis of unpolished detrital zircons recovers $^{206}Pb/^{238}U$ and $^{207}Pb/^{235}U$ isotopic data during progressive laser-ablation penetration. Washout experiments have demonstrated that depth profiling allows recovery of robust age data from <0.25 μm depth intervals (e.g., Smye and Stockli, 2014). After downhole- and mass-fractionation correction, depth-profile data can be parsed into different concordant age domains and interpreted as either a single age domain or multiple discrete growth zones (e.g., rim and core). This methodology allows for systematic recovery of multiple growth zones from individual detrital zircons, enabling refined provenance interpretations and the exploration of potential genetic relationships between different zircon U-Pb age modes (e.g., Liu et al., 2022). In this study, only 101 rim ages were observed out of 4246 total analyses (2.4%).

A Photon Machines Analyte G2 excimer laser with a HelEx sample chamber attached to a Thermo Element2 ICP-MS was utilized for U-Pb LA-ICP-MS analyses. We utilized GJ1 as the primary reference material (601.7 ± 1.3 Ma; Jackson et al., 2004) for depth-hole and elemental fractionation and Plešovice (337.13 ± 0.37 Ma; Sláma et al., 2008) as the secondary reference material to quantify the reproducibility of the analyses. Propagated errors calculated using a VizualAge data reduction scheme are reported. No common Pb correction was applied, and the presence of zircon overgrowths was not verified by cathodoluminescence imaging prior to or after grain analysis. For detrital zircon U-Pb dates younger than 850 Ma, the $^{206}Pb/^{238}U$ dates are reported as the best U-Pb age, and for dates older than 850 Ma, the $^{207}Pb/^{206}Pb$ date is reported as the best U-Pb age. This age transition occupies a natural break in grain ages in the data set between grains in the range 1320–900 Ma and younger Neoproterozoic grains. Data filters for a $^{206}Pb/^{238}U$ error limit of 10%, a $^{206}Pb/^{238}U$ versus $^{207}Pb/^{235}U$ discordance limit of 30%, and a $^{206}Pb/^{238}U$ versus $^{207}Pb/^{206}Pb$ limit of 30% were utilized to remove zircon with large uncertainties and high discordance.

An attempt was made to analyze at least 120 zircon grains per sample to ensure recovery of grain age groups representing more than 5% of the total sample population (Vermeesch, 2004), but analyses in our data set ranged from a high of 145 to a low of 71 from a sand-poor site. Kernel density estimator (KDE) plots, a multidimensional scaling plot, and a core-rim age-pair plot were generated using algorithms in detritalPy, a Python-based toolkit for manipulating large geochronology data sets (Sharman et al., 2018). Because the true depositional age of the samples in our data set is known to be approximately 0 Ma (e.g., Sharman and Malkowski, 2020), we present maximum depositional age (MDA) estimates for each sample to provide insight as to accuracy of these estimates in our set of modern sand samples. MDA values were determined both from the youngest single grain age (YSG; Dickinson and Gehrels, 2009b) and from multigrain estimates calculated employing the weighted mean algorithm in Isoplot 3.00 (Ludwig, 2003) of the youngest age mode for which a cohort ($n \geq 2$) of grain ages overlapped at 2σ uncertainty. These MDA values are listed in Table 1.

PHYSIOGRAPHIC AND GEOLOGIC SETTING

This study considered the western coastline of the Gulf of Mexico and rivers draining to it from the mouth of the Rio Grande (Río Bravo del Norte if viewed from the south) to the mouth of Río La Antigua, 20 km north of the city of Veracruz, Mexico, representing a span of ~750 km (Fig. 2). Many states and their state capitals in Mexico are eponymous; to avoid confusion as to geography, proper names in the text refer to states rather than the cities within them unless otherwise stipulated.

Beaches

The northern part of the Mexican coastline lies outboard of a broad fluvial coastal plain flanked by an extensive system of back-barrier bays, the Laguna Santa Maria, and a continuous strand plain that extends south to the mouth of the Río Soto La Marina at La Pesca, in the coastal state of Tamaulipas. Southward from there, the coastal plain is flanked by exposed, seaward-dipping Paleogene–Neogene strata, and the strandline lacks major bays except near Tampico, at the mouth of the Río Pánuco, which marks the southern border of Tamaulipas. In adjacent Veracruz, the coastal plain extends inland across irregular low-lying topography of folded Paleogene strata to an abrupt escarpment composed dominantly of limestone at the east flank of the Sierra Madre Oriental. The coastal plain narrows southward and is effectively absent where basaltic lava flows of the Eastern Alkaline volcanic province (Ferrari et al., 2005) in the eastern part of the Trans-Mexican volcanic belt encroach upon the coastline. South of the Trans-Mexican volcanic belt, the coastal plain widens abruptly where it encounters the Veracruz basin.

Fluvial Catchments

Rivers of the study area were divided into four groups, which included the Rio Grande and rivers of the Río San Juan catchment in northeastern Mexico that drain to the lower Rio Grande, rivers of Nuevo León and Tamaulipas draining to the northwestern Gulf of Mexico, the Río Pánuco catchment, and Veracruz catchments. Drainage basin areas, annual discharges, and climatic regimes of selected rivers are shown in Figure 3.

Rio Grande–Río San Juan Catchments

The Rio Grande watershed is the largest catchment that contributes sediment to the Gulf of Mexico considered in this study. The greater Rio Grande watershed encompasses 870 × 10^3 km^2 (Milliman and Farnsworth, 2011) with a principal trunk stream that heads in Paleogene volcanic rocks of the San Juan volcanic field of southwestern Colorado and flows southward along the Rio Grande rift in Colorado and New Mexico. In the northern part of the rift, the river crosses an edge of the small but significant Jemez Mountains volcanic field, dominated by Pleistocene rhyolitic ignimbrites (Goff and Gardner, 2004). The main tributaries of the Rio Grande in the rift include the Chama, Puerco, and Salado Rivers, which enter the main river from the west and drain mostly Paleozoic and Mesozoic sedimentary rocks of the Colorado Plateau (Fig. 1). The principal tributary of the Rio Grande in the United States is the Pecos River, with a drainage basin area of 115 × 10^3 km^2, draining the southern Rocky Mountains of New Mexico and Colorado. A significant part of the Rio Grande catchment (68.4 × 10^3 km^2) is represented by the Río Conchos of Chihuahua, which drains the high volcanic plateau of the Sierra Madre Occi-
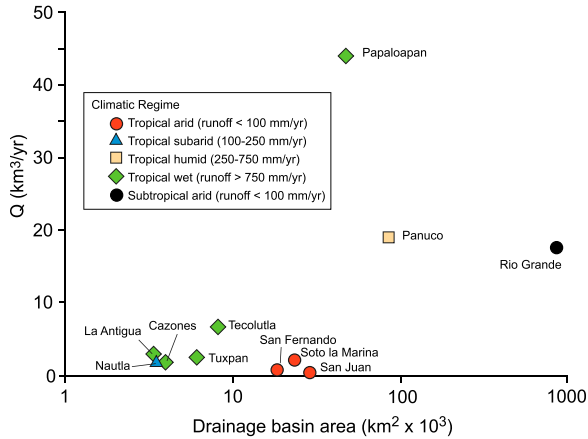
Figure 3. River basin plot of catchment area vs. discharge (*Q*) and dominant climatic regime of the watershed after Milliman and Farnsworth (2011). Río Papaloapan, in southeasternmost part of Figure 2, was not sampled as part of this study.

dental. The lower Rio Grande receives discharge from the Río San Juan catchment (68.4×10^3 km²), which includes the trunk stream, sampled in its upper reach, and two sampled tributaries, Río Ramos and Río Pilón, in southeastern Nuevo León. These rivers drain uplifted Mesozoic strata of the Sierra Madre Oriental. Ephemeral tributaries within the San Juan catchment in Nuevo León north of the Sierra Madre Oriental (Fig. 2) cross Upper Cretaceous and Paleogene siliciclastic sedimentary rocks; although ephemeral, these arid-climate drainages are characterized by extreme discharge events during the passage of tropical depressions and hurricanes over northeastern Mexico. All large tributaries of the Rio Grande in the United States and Mexico and the main stream itself have major dams for water storage and hydroelectric production. We sampled low-water sandbars of the Rio Grande (17RG01, 17RG02) from the lower part of the river near Brownsville, Texas (Fig. 2), below the confluence of the Río San Juan and approximately 50 km upstream of the river mouth; we also utilized previously published data for modern sand of the Rio Grande from two samples collected farther upriver at Laredo, Texas (Fig. 2; Blum et al., 2017; Fan et al., 2019).

Catchments Draining Directly to the Northwestern Gulf of Mexico

Two watersheds in northeastern Mexico contain perennial tropical arid rivers that flow directly from the Sierra Madre Oriental to the Gulf of Mexico. These include the Río Pablillo in southern Nuevo León, which becomes the Río San Fernando of Tamaulipas, with a catchment area of 18×10^3 km², the Río Soto La Marina of Tamaulipas, with a catchment area of 23×10^3 km², and the Río Purificación, a principal tributary to the Soto La Marina in central Tamaulipas that drains directly from uplifted carbonate strata of the Sierra Madre Oriental. The tributaries of this region are ephemeral and

characterized by high-discharge events during passage of subtropical depressions during summer and autumn months. We sampled the Río Pablillo (17NEMX05) and Río Purificación (17NEMX06) (Fig. 2).

Río Pánuco Catchment

The Río Pánuco watershed, at 85×10^3 km², is the second largest catchment draining to the western Gulf of Mexico, after the Rio Grande, which has an order-of-magnitude larger watershed (Milliman and Farnsworth, 2011). Classified as a tropical humid river, the estimated annual discharge of the Río Pánuco is 19 km³/yr (Fig. 3; Milliman and Farnsworth, 2011). The catchment drains the northern half of the Huayacocotla uplift, which contains local exposures of Grenville basement, a Permian volcano-sedimentary section, and Jurassic sedimentary strata, as well as an extensive Cretaceous–Paleogene section of the Sierra Madre Oriental and Upper Eocene–Oligocene pyroclastic rocks of a southeastward extension of the Sierra Madre Occidental volcanic field. Major trunk rivers, including the Río Amajac and Río Moctezuma, tap Miocene and younger volcanic rocks of the Trans-Mexican volcanic belt (Fig. 2). Tributaries of the southern and central parts of the Río Pánuco catchment are well represented by samples in this study (Fig. 2; Table 1). We collected samples from the Ríos Moctezuma, Amajac, and Tamuin, and second-order tributaries of the Ríos Calabozo, Atlapexco, and Garces. The Río Tamuin, the northernmost river sampled in the catchment, joins the Río Moctezuma at the San Luis Potosí–Veracruz state line. The Ríos Calabozo, Atlapexco, and Garces join the Río Moctezuma via the Río Tempoal at El Higo, Veracruz. The name Pánuco only applies to the trunk river downstream of the confluence of the Ríos Moctezuma and Tamuin (Hudson, 2003); we were unable to collect a sand sample from the Río Pánuco itself because sand bars were submerged.

Veracruz Catchments

Transverse rivers of Veracruz drain the eastern part of the Sierra Madre Oriental, with increasing influence of the Trans-Mexican volcanic belt southward, and cross the narrow coastal plain of the Gulf of Mexico. These perennial rivers are considered tropical arid to tropical wet with elevation-dependent rainfall and greatest precipitation in August and September, which results in high-discharge events (Self, 1977). From north to south, three of these, the Ríos Vinazco, Pantepec, and Cazones, principally cut canyons in sedimentary and local basement rocks of the Sierra Madre Oriental and cross mafic volcanic flows of the eastern Trans-Mexican volcanic belt. The Río Tecolutla, which lacks dams, has headwaters in the northeastern part of the Trans-Mexican volcanic belt (eastern sector of Ferrari et al., 2005, 2007) within 40 km of an active stratovolcano, La Malinche, on the Tlaxcala-Puebla state line (Fig. 2). The Río Nautla likewise heads in the eastern sector of the Trans-Mexican volcanic belt, draining to the Gulf of Mexico north of the volcanic belt. The southernmost river sampled for this study, the Río La Antigua, lacks dams and has headwaters on the eastern slopes of the highest point in Mexico, Pico de Orizaba or Citlaltépetl, an inactive stratovolcano. We also collected one or more samples from each of the Ríos Vinazco, Pantepec, Cazones, Tecolutla, and Nautla (Table 1; Fig. 2).

SOURCES OF ZIRCON GRAINS IN EAST-DRAINING MEXICAN RIVERS

Zircon originates in intermediate to felsic melts and can be newly generated or added as overgrowths to existing zircon crystals during metamorphism or incorporation into younger igneous melts (Corfu et al., 2003; Hoskin and Schaltegger, 2003). Due to its resistance to chemical and mechanical weathering, zircon is particularly susceptible to recycling from previously deposited sandstone (e.g., Dickinson et al., 2009; Lawton et al., 2010). Therefore, a review of potential sources, both primary and recycled, for zircon in the catchments that drain to the eastern Gulf of Mexico is included in this section. These sources are listed in Table 2.

Sierra Madre Occidental and Trans-Pecos Volcanic Field

The Oligocene Sierra Madre Occidental volcanic field is a silicic large igneous province (Ferrari et al., 2005, 2007) that extends over 1000 km north-south along the western flank of Mexico (Fig. 1). An Oligocene–lower Miocene segment of the volcanic field forms an east-trending outcrop belt from the southern Sierra

TABLE 2. INFERRED SOURCES OF PRINCIPAL DEFINED AGE GROUPS, SOUTHWESTERN UNITED STATES AND NORTHERN MEXICO

Age group (Ma)	Modal ages (Ma)	Tectonic/igneous unit	Principal sources	Reference
3000–2300	No significant modes	Wyoming provinces	N Rocky Mountains	Whitmeyer and Karlstrom (2007)
		Superior province	NE North America	Whitmeyer and Karlstrom (2007)
1800–1500 (Statherian–Calymmian)	Ca. 1706–1687, 1542	Yavapai-Mazatzal basement	S Rocky Mountains	Whitmeyer and Karlstrom (2007)
1500–1320 (mainly Calymmian)	1433, 1431 1423, 1406	Granite-Rhyolite plutons	S Rocky Mountains	Whitmeyer and Karlstrom (2007)
1320–900 (Ectasian–Tonian)	Various ranging 1319–953	Grenville basement of Oaxaquia (Eastern Mexico)	Basement of Huayacocotla uplift Jurassic–Paleogene strata of SMO	Lawlor et al. (1999) Ortega-Flores et al. (2014); Juárez-Arriaga et al. (2019a, 2019b)
850–550 (middle Tonian–Ediacaran)		Neoproterozoic (Pan-African) basement of peri-Gondwanan terranes, especially Maya block, likely recycled	Triassic and Jurassic rift strata of SMO	Barboza-Gudiño et al. (2010); Martin et al. (2022)
500–328 (Paleozoic)	416	Famatinian arc, West Pangea arc	Paleozoic intrusions of SMO	Alemán-Gallardo et al. (2019)
295–200 (Permian–Triassic)	295, 286, 283 276–269, 256	West Pangea arc "East Mexico arc"	Permian volcanic rocks of SMO	Rosales-Lagarde et al. (2005) Dickinson and Lawton (2001)
200–110 (Jurassic–Early Cretaceous)	No significant modes	Jurassic–Early Cretaceous magmatism	Upper Cretaceous strata of SMO	Juárez-Arriaga et al. (2019a, 2019b)
110–55 (late Early Cretaceous–early Eocene)	Ca. 84, 79, 74 89, 75, 56	Late Cretaceous–Paleogene arc	Upper Cretaceous strata of SMO	Velasco-Tapia et al. (2016) Juárez-Arriaga et al. (2019a, 2019b)
55–20 (Eocene–Oligocene)	Ca. 33–31	Paleogene volcanic and volcaniclastic rocks	SMO SLIP; Trans-Pecos volcanic field	Ferrari et al. (2007)
	Ca. 33–32			Cepeda and Henry (1983)
	Ca. 36–27		Mogollon-Datil volcanic field, NM	McIntosh et al. (1992); Chapin (2012)
	Ca. 36–26		San Juan volcanic field	Lipman and McIntosh (2008); Chapin (2012)
	Ca. 31–27 (K-Ar)		Tamaulipas intrusive complex	Ortega-Gutiérrez et al. (2014)
	Ca. 32–30		Mesa Central	Díaz-Bravo et al. (2022)
20–0 (Miocene–recent)	13, 3, 2	Mexican Neogene arc	TMVB	Ferrari et al. (2012)
	Ca. 7		Eastern Trans-Mexican volcanic belt	Gómez-Alvarez et al. (2021)
	Ca. 5.3–2.6, 1.6–1.2 (Ar-Ar)	Jemez Mountains volcanic field (northern New Mexico)	Rio Grande rift	Spell et al. (1996); Nasholds and Zimmerer (2022)
	Ca. 0.019-0.006 (Ar-Ar)	Active volcanoes in Trans-Mexican volcanic belt	TMVB	Chako Tchamabé et al. (2020)

Notes: SMO—Sierra Madre Oriental; SLIP—silicic large igneous province; NM—New Mexico; TMVB—Trans-Mexican volcanic belt.

Madre Occidental volcanic field to the east-central part of San Luis Potosí (Ferrari et al., 2007; Díaz-Bravo et al., 2022). The headwaters of the Río Pánuco catchment reach this part of the Sierra Madre Occidental volcanic field. The Río Conchos of north-central Mexico also drains from the Sierra Madre Occidental volcanic field to join the Rio Grande upstream of the Big Bend in west Texas, and thus also transports sediment derived from the volcanic field.

The Sierra Madre Occidental volcanic field consists of five igneous complexes ranging in age from Cretaceous to early Miocene (Ferrari et al., 2007): (1) an assemblage of Upper Cretaceous–Paleogene plutonic rocks that constitute part of the older Mexican Cordilleran arc (Juárez-Arriaga et al., 2019a); (2) Eocene andesites and subordinate rhyolites; (3) voluminous silicic ignimbrites that were emplaced in two phases during the Oligocene (32–28 Ma) and latest Oligocene–early Miocene (24–20 Ma), with the latter dominantly occupying the southeastern part of the volcanic field; (4) transitional basaltic-andesitic lava flows erupted near the end of, and after, each episode of ignimbrite eruptions; and (5) postsubduction alkaline basalts and ignimbrites of late Miocene, Pliocene, and Pleistocene age, formed during separation of the Baja California Peninsula from western Mexico.

We expect that the Eocene volcanics, Oligocene–Upper Miocene ignimbrites, and Neogene small-volume ignimbrites contributed the bulk of the zircons from the Sierra Madre Occidental volcanic field.

The Trans-Pecos volcanic field, a northeastern extension of the Sierra Madre Occidental volcanic field (Fig. 1), is a deeply eroded complex of calderas and silicic ignimbrites that lies directly west of the Big Bend in western Texas. The Rio Grande and small tributaries draining into the trunk river from the north traverse the volcanic field. Volcanic and volcaniclastic rocks of the Trans-Pecos volcanic field range from 33 Ma to 32 Ma (Cepeda and Henry, 1983), making them indistinguishable in age from the Oligocene ignimbrites of the Sierra Madre Occidental volcanic field.

Sierra Madre Oriental

Mesozoic to Cenozoic siliciclastic and carbonate strata make up most of the exposed rocks in the fold-and-thrust belt of the Sierra Madre Oriental. Zircon grains derived from this physiographic province likely include many grains recycled from sedimentary strata rather than derived from primary sources. Nevertheless, deep canyons in Tamaulipas, Hidalgo, and Vera-cruz expose older rocks, including: (1) Grenville Huiznopala Gneiss, which consists of orthogneisses and metasedimentary rocks ranging 1320–900 Ma in age (Fig. 1; Lawlor et al., 1999; Ortega-Gutiérrez et al., 2014); (2) Lower Paleozoic metagranitoids of the Huizachal uplift in Tamaulipas and Nuevo León (Alemán-Gallardo et al., 2019); (3) Lower Permian volcanic and volcano-sedimentary rocks (Rosales-Lagarde et al., 2005); and (4) Triassic and Jurassic rift-related strata and volcanic rocks derived from Proterozoic basement and Paleozoic rocks, as well as Permian–Triassic plutons in the basement of the Tamaulipas arch (Barboza-Gudiño et al., 2010; Rubio-Cisneros and Lawton, 2011). Uncommon zircon grains derived from Neoproterozoic rocks of peri-Gondwanan affinity (ca. 850–550 Ma) also occur in Triassic and Jurassic strata of the Sierra Madre Oriental (Barboza-Gudiño et al., 2010; Martin et al., 2022). The original source for these grains was likely Pan-African basement of the Maya block (e.g., Ross et al., 2022), now largely covered by younger carbonate strata of the Yucatán Peninsula and Campeche Bank. Fine-grained strata of the Caracol and San Felipe Formations of the Sierra Madre Oriental contain numerous tuff beds in the range ca. 85–74 Ma derived from eruptions of a Cretaceous magmatic arc in western Mex-

ico (Velasco-Tapia et al., 2016; Juárez-Arriaga et al., 2019a).

Trans-Mexican Volcanic Belt

The Trans-Mexican volcanic belt, a volcanic field that spans Mexico from the Pacific margin to the Gulf of Mexico (Fig. 1), developed during four magmatic episodes (Ferrari et al., 2012): (1) From ca. 20 Ma to 10 Ma, an initial andesitic arc migrated northward away from the trench, followed by migration to approximately its current position near the end of the Miocene (Ferrari et al., 2007, fig. 1); (2) since ca. 11 Ma, a pulse of mafic magmatism migrated eastward, to reach the Gulf of Mexico by 7 Ma; (3) a phase of silicic magmatism from 7.5 to 3 Ma was characterized by trenchward migration of the volcanic front and local emplacement of intraplate basalts beginning 5 Ma; and (4) a modern arc has a southern frontal belt composed of intermediate and mafic rocks and a northern inner belt composed of differentiated rocks or mafic lavas. The magmatic history suggests zircon ages derived from the Trans-Mexican volcanic belt should begin about 20 Ma, with principal zircon production at 7.5–3 Ma.

RESULTS

Sand Petrography

Modal point counts demonstrated that sand compositions within the study area vary significantly from north to south, the direction in which they are described in the text (Fig. 4).
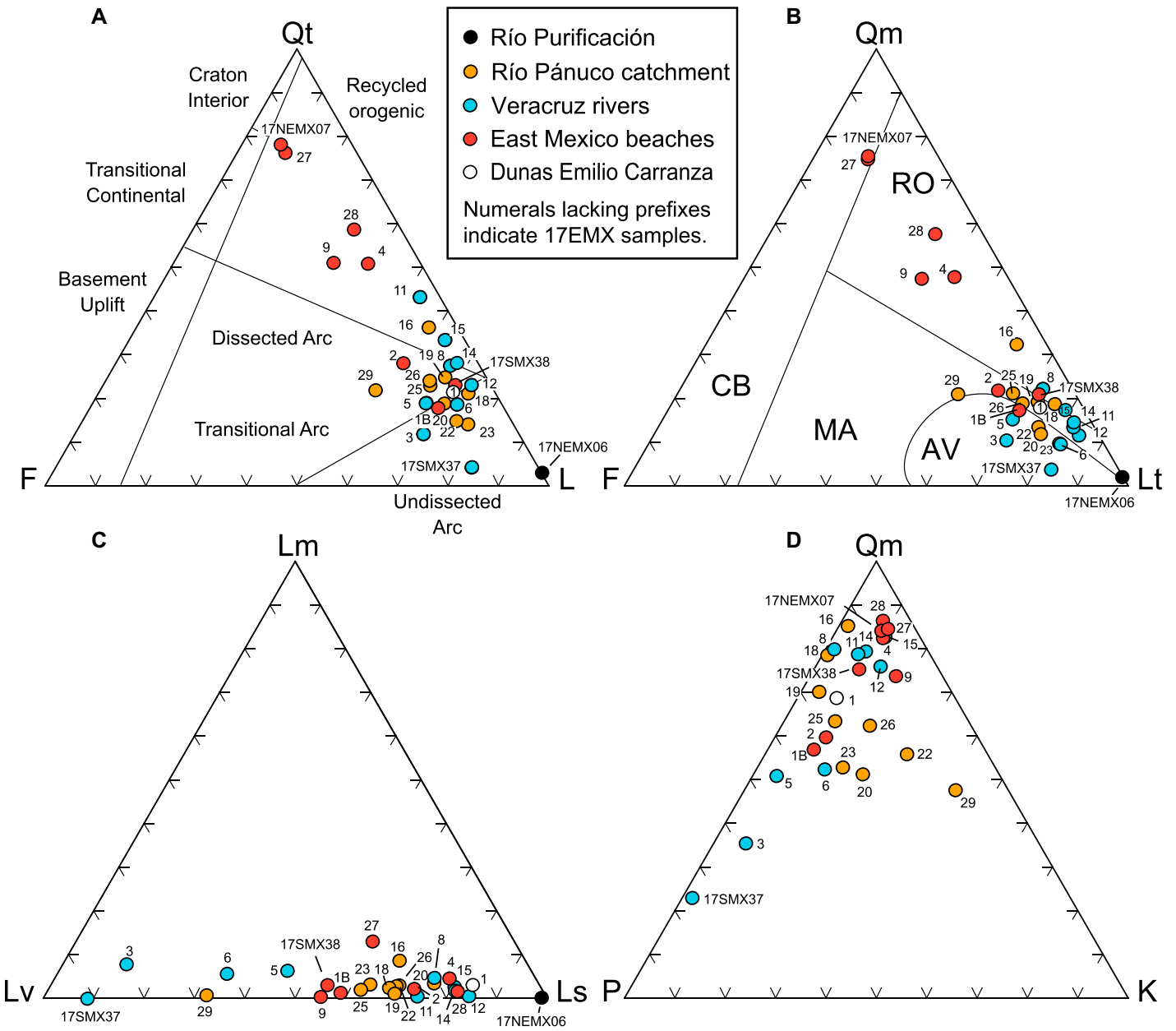
Figure 4. Ternary plots of sands from eastern Mexico rivers and beaches. (A) QtFL plot. Provenance fields are from Dickinson (1985). (B) QmFLt plot. Provenance fields are from Garzanti (2016). AV—anorogenic volcanic; CB—continental block; MA—magmatic arc; RO—recycled orogen. (C) LmLvLs plot. (D) QmPK plot. Plot symbols are explained in more detail in Tables 3 and 4.

TABLE 3. POINT COUNT SYMBOL DEFINITIONS AND RECALCULATED PARAMETERS

Symbol	Definition
Point count symbol definitions	
Qm	Monocrystalline quartz
Qp	Polycrystalline quartz (= microcrystalline chert + foliated quartz aggregates + aggregates with mosaic texture)
K	Potassium feldspar
P	Plagioclase feldspar
Lv	Volcanic lithic grains (= felsitic [Lvf] + vitric [Lvv] + microlitic [Lvmi] + lathwork [Lvl] grains)
Lm	Metamorphic lithic grains: quartz-mica aggregates, some with foliated texture
Ls	Sedimentary lithic grains (= extrabasinal carbonate [Lsc] + siltstone [Lss] + argillite [Lss] grains)
Qt	Total quartzose grains (= Qm + Qp)
F	Total feldspar (= K + P)
L	Total unstable lithic grains (= Lv + Lm + Ls)
Lt	Total lithic grains (= L + Qp)
Recalculated parameters of Table 4	
$QtFL\%Qt = 100Qt/(Qt + F + L)$	
$QtFL\%F = 100F/(Qt + F + L)$	
$QtFL\%L = 100L/(Qt + F + L)$	
$QmFLt\%Qm = 100Qm/(Qm + F + Lt)$	
$QmFLt\%F = 100F/(Qm + F + Lt)$	
$QmFLt\%Lt = 100Lt/(Qm + F + Lt)$	
$QmKP\%Qm = 100Qm/(Qm + K + P)$	
$QmKP\%K = 100 K/(Qm + K + P)$	
$QmKP\%P = 100P/(Qm + K + P)$	
$LmLvLs\%Lm = 100Lm/(Lm + Lv + Ls)$	
$LmLvLs\%Lv = 100Lv/(Lm + Lv + Ls)$	
$LmLvLs\%Ls = 100Ls/(Lm + Lv + Ls)$	
$LvfLvmiLvl\%Lvf = 100Lvf/(Lvf + Lvmi + Lvl)$	
$LvfLvmiLvl\%Lvmi = 100Lvmi/(Lvf + Lvmi + Lvl)$	
$LvfLvmiLvl\%Lvl = 100Lvl/(Lvf + Lvmi + Lvl)$	
$LvvLvmiLvl\%Lvv = 100Lvv/(Lvv + Lvmi + Lvl)$	
$LvvLvmiLvl\%Lvmi = 100Lvmi/(Lvv + Lvmi + Lvl)$	
$LvvLvmiLvl\%Lvl = 100Lvl/(Lvv + Lvmi + Lvl)$	

Principal grain types and point counting parameters are listed in Table 3, and recalculated modal point count data are presented in Table 4. Brief descriptions of samples and raw point count data of individual samples are listed in Table S1[1]. Names of compositionally related sediment suites in the following sections are descriptive terms devised by Garzanti (2016), determined from our QmFLt plot (Fig. 4A), which most closely employed the recalculated parameters of Garzanti (2016).

Sedimentary Lithic Sands in Rivers of Nuevo León and Tamaulipas

Our single petrographic sand sample (17NEMX06) of a petrofacies composed of sedimentary lithic fragments (Ls) came from the Río Purificación in central Tamaulipas. It was fine- to medium-grained lithic sand with a modal composition of $Qt_3F_0L_{97}$ (Table 4), in which 99% of the lithic grains were finely crystalline detrital carbonate grains (Lsc of Ingersoll et al., 1987), commonly containing fossils that

included foraminifera and bryozoans. Uncommon felsitic volcanic grains (Lvf; ~1%) and chert (~1%) were present, and a single plutonic rock fragment consisting of quartz and alkali feldspar was observed.

Quartzo-Lithic and Feldspatho-Quartzo-Lithic River Sands of the Río Pánuco Catchment

Sands of rivers in the Río Pánuco catchment consisted of moderately to poorly sorted, fine- to very coarse-grained sand with angular to subrounded grains. The sands had a limited range of quartzo-lithic and quartzo-feldspatho-lithic compositions from $Qm_{10}F_9Lt_{81}$ to $Qm_{33}F_6Lt_{62}$ (mean = $Qm_{19}F_{11}Lt_{71}$; Fig. 4B; Table 4). On average, sedimentary lithic grains (LmLvLs%Ls mean = 64%) were more abundant than volcanic lithic fragments (LmLvLs%Lv mean = 33%), and metamorphic lithic fragments (Lm) did not exceed 9% (Fig. 4C).

Lithic sands from different watersheds of the Río Pánuco catchment varied significantly in terms of lithic fragment composition. Samples from the Ríos Amajac and Moctezuma contained a diverse mixture of Lv types, including felsitic grains and uncommon lathwork grains with intergranular to intersertal textures consisting of plagioclase laths with small crystals of olivine. Detrital carbonate grains, mostly consisting of microcrystalline textures with foraminifera and other microfossils, were common

to abundant. Chert was common, particularly in the Río Moctezuma samples, and one sample (17EMX23) from a high-water, predam sandbar contained 1%–2% glassy fragments, some as pumiceous domains in Lvf fragments, and some as individual, sickle-shaped isotropic shards. A single sample from the Río Tamuin (17EMX29) contained abundant feldspar, mostly alkali feldspar, and was dominated by volcanic lithic fragments (LmLvLs%Lv = 69%; Table 4). Most Lv consisted of felsitic (Lvf) grains (LvfLvmiLvl%Lvf = 79%), some with eutaxitic texture, indicating derivation from silicic volcanic and pyroclastic rocks (Figs. 5A and 6; Table 4; Marsaglia and Ingersoll, 1992). Molluscan fragments, evidently pieces of freshwater clams, constituted 1%–2% of most samples.

Sands contributed via the Río Tempoal watershed were compositionally different from the northern rivers of the Pánuco catchment. Sands of the three tributary rivers were poorly sorted, angular to subrounded, and very fine to medium grained in the range 0.1–1.0 mm (Fig. 5B). They contained less feldspar (6%) and fewer volcanic lithic fragments (LmLvLs%Lv average = 28%) than the other samples of the Río Pánuco catchment (Table 4). All samples contained distinctive Lss grains represented by hematitic coarse angular siltstone with quartzo-lithic composition and mica in some grains; these grains made up roughly half of the Ls fraction in the Ríos Garcés and Atlapexco samples and were the dominant Ls grain type in the Río Calabozo. Volcanic lithic grains included common Lvl, with some grains containing weathered ferro-magnesian minerals and others consisting of fresh basaltic grains with subophitic to intergranular textures of large aligned plagioclase crystals and fresh olivine grains. Lsc and chert were common; Lm grains, consisting of granular quartz and mica, were uncommon. The Río Calabozo sample (17EMX19) notably contained coarse molluscan fragments.

Lithic Sands of Veracruz Rivers

Transverse rivers of Veracruz transport sand that is universally angular to subrounded and poorly sorted, with grain sizes ranging from fine to very coarse. Sands of the Veracruz rivers ranged from quartzo-lithic to feldspatho-quartzo-lithic compositions, on average richer in volcanic lithic fragments than rivers of the Río Pánuco catchment (mean = $Qm_{13}F_8Lt_{79}$; Fig. 4; Table 4). Although mean lithic content was not significantly different from sands of the Río Pánuco catchment, LmLvLs%Lv ranged from 15% to 91%. LmLvLs%Lm was consistently low, with a maximum value of 8%.

Lithic grain types, abundant in all Veracruz rivers, changed southward along the coastal

TABLE 4. RECALCULATED MODAL POINT COUNT DATA FOR MODERN RIVER AND BEACH SANDS, EASTERN MEXICO

Sample	River/beach	QtFL%			QmFLt%			LmLvLs%			QmPK%			LvfLvmiLvl%			LvvLvmiLvl%		
		Qt	F	L	Qm	F	Lt	Lm	Lv	Ls	Qm	P	K	Lvf	Lvmi	Lvl	Lvv	Lvmi	Lvl
Tamaulipas river																			
17NEMX06	Río Purificación	3	0	97	2	0	98	0	1	99	N.A.	N.A.	N.A.	N.A.	N.A.	N.A.	N.A.	N.A.	N.A.
Río Pánuco catchment																			
17EMX19	Río Calabozo	25	8	67	20	8	72	1	29	69	70	26	4	N.A.	N.A.	N.A.	N.A.	N.A.	N.A.
17EMX16	Río Garcés	36	6	58	33	6	62	9	25	67	85	13	2	N.A.	N.A.	N.A.	N.A.	N.A.	N.A.
17EMX18	Rio Atlapexco	21	5	74	19	5	76	2	30	68	78	21	1	N.A.	N.A.	N.A.	N.A.	N.A.	N.A.
17EMX29	Río Tamuin	22	23	55	21	23	56	1	67	32	48	10	42	79	10	11	0	52	48
17EMX20	Río Amajac	19	11	70	12	11	77	4	21	76	51	27	22	N.A.	N.A.	N.A.	N.A.	N.A.	N.A.
17EMX22	Río Moctezuma	15	11	74	14	11	76	3	28	69	56	16	28	N.A.	N.A.	N.A.	N.A.	N.A.	N.A.
17EMX23	Río Moctezuma	14	9	77	10	9	81	3	34	63	53	30	17	85	13	2	58	6	35
17EMX25	Río Moctezuma	23	12	65	21	12	67	2	36	62	63	26	10	72	18	9	25	25	50
17EMX26	Río Moctezuma	24	12	64	19	12	69	3	28	69	62	20	18	N.A.	N.A.	N.A.	N.A.	N.A.	N.A.
Mean		22	11	67	19	11	71	3	33	64	63	21	16						
Std dev		6	5	7	7	5	8	2	13	12	13	7	14						
Veracruz rivers																			
17EMX15	Río Vinazco	33	4	63	17	4	79	2	17	80	82	7	11	N.A.	N.A.	N.A.	N.A.	N.A.	N.A.
17EMX12	Río Pantepec	23	4	73	12	4	85	0	15	84	76	11	13	N.A.	N.A.	N.A.	N.A.	N.A.	N.A.
17EMX14	Río Pantepec	28	4	68	14	4	82	2	18	81	79	13	8	N.A.	N.A.	N.A.	N.A.	N.A.	N.A.
17EMX11	Río Pantepec	43	4	53	14	4	83	0	26	74	79	14	7	N.A.	N.A.	N.A.	N.A.	N.A.	N.A.
17EMX08	Río Cazones	27	6	67	22	6	72	5	20	75	80	18	2	N.A.	N.A.	N.A.	N.A.	N.A.	N.A.
17EMX06	Río Tecolutla	19	9	73	9	9	82	6	61	34	52	34	14	61	27	12	62	12	27
17EMX05	Río Tecolutla	19	15	67	15	15	70	6	49	45	51	44	5	56	22	22	64	18	18
17EMX03	Río Nautla	12	19	70	10	19	71	8	79	13	35	58	7	27	33	40	63	20	17
17SMX37	Río La Antigua	4	13	84	4	13	84	0	91	9	23	76	2	3	44	53	7	51	42
Mean		23	8	69	13	8	79	3	42	55	62	31	8						
Std dev		12	6	8	5	6	6	3	29	30	22	24	4						
Eastern Mexico beaches																			
17NEMX07	La Pesca, Tamaulipas	79	14	8	76	14	11	N.A.	N.A.	N.A.	84	7	9	N.A.	N.A.	N.A.	N.A.	N.A.	N.A.
17EMX27	Playa Miramar, N of Río Pánuco mouth	76	14	10	75	14	11	13	28	59	84	6	10	N.A.	N.A.	N.A.	N.A.	N.A.	N.A.
17EMX28	Playa Hermosa, S of Río Pánuco mouth	59	9	32	58	9	33	1	17	82	86	6	8	N.A.	N.A.	N.A.	N.A.	N.A.	N.A.
17EMX09	Playa Tuxpan, N of river mouth	51	17	32	48	17	36	0	45	55	74	9	17	N.A.	N.A.	N.A.	N.A.	N.A.	N.A.
17EMX04	Beach at Tecolutla, Veracruz	51	10	39	48	10	42	4	17	78	82	8	10	N.A.	N.A.	N.A.	N.A.	N.A.	N.A.
17EMX02	Beach at Nautla, Veracruz	28	15	57	22	15	63	2	25	73	60	30	10	N.A.	N.A.	N.A.	N.A.	N.A.	N.A.
17EMX01	Dunes at Emilio Carranza	21	8	71	18	8	74	3	13	84	69	23	8	N.A.	N.A.	N.A.	N.A.	N.A.	N.A.
17EMX01B	Beach at Santa Ana, Veracruz	18	13	69	17	13	70	1	40	59	57	34	9	14	50	35	0	41	59
17SMX38	Playa Chachalacas, Veracruz	23	7	70	21	7	72	3	42	55	76	16	9	35	55	10	0	15	85
Mean		45	12	43	42	12	46	4	28	68	75	15	10						
Std dev		24	3	25	24	3	25	4	12	12	11	11	3						

Notes: Total quartz (Qt) = monocrystalline quartz (Qm) + polycrystalline quartz (Qp); rare chert is included Qp grain category. Total feldspar (F) = alkali feldspar (K) + plagioclase (P). L—microcrystalline lithic fragments. Total lithic fragments (Lt) = L + Qp. Lm—metamorphic lithic fragments; Ls—sedimentary lithic fragments; Lv—volcanic lithic fragments. Lv is subdivided as follows: Lvv—vitric grains; Lvm—microlitic grains, Lvl—lathwork grains. N.A.—not calculated for samples with normalized modal percentage totals with QtFL%L < 20% or Lv total <20% of modal counts. See Table S1 for count totals (see text footnote 1).

plain (Table 4). Sedimentary lithic fragments (Ls) dominated samples of the Ríos Vinazco and Pantepec, which had abundant Lsc and common Lss grains, the latter consisting of coarse hematitic siltstone with angular quartz grains and abundant carbonate grains or clay. Some Lsc grains contained fossils. Chert grains, commonly with radiolaria, were abundant in some samples (Fig. 5C). Fresh basaltic Lvl grains displayed subophitic and intergranular textures. Lv grains, particularly Lvl, were prominent in sand of the Río Cazones (17EMX08) (Fig. 6A), which contained 1%–2% blocky colorless glass fragments (Lvv) and lesser amounts of Lsc and chert grains. Vitric volcanic grains (Lvv) were an important component of sand in the Ríos Tecolutla and Nautla samples (17EMX05, 17EMX06, and 17EMX03; Fig. 6B). Fragments

of volcanic glass, including blocky angular grains with partial spherical vesicles, spindle-shaped shards, and antler-like multipronged combs, were common in samples of the Río Tecolutla (Fig. 5D), where Lvv grains ranged as high as 17% of counted grains. Other diverse Lv grains, including fresh Lvl and Lvmi grain types with altered glassy groundmass, were abundant. Foliated quartz-mica Lm grains were uncommon. A sand sample from the Río Nautla (17EMX03) also contained abundant colorless to pale brown volcanic glass grains (39% of grains counted) with textures ranging from delicate acicular shapes and frothy pumice to blocky fragments with partial vesicles. Our point count from the Río Nautla ($Qt_{12}F_{19}L_{70}$) compares favorably with grain proportions ($\sim Qt_{25}F_{13}L_{62}$) previously reported by Self

(1975) from the lower part of the river, including abundant grains described as ash fragments (our Lvv) and proportionately fewer grains described as limestone rock fragments (our Lsc) (Self, 1975).

The sample (17SMX37) containing the most volcanic lithic grains (LmLvLs%Lv = 91%) came from Río La Antigua, the southernmost sampled river of this study. It contained a diverse assortment of monocrystalline plagioclase and accessory Fe-Mg silicate grains including clinopyroxene, olivine, and bright reddish-brown hornblende, which made up ∼20% of grains, and unaltered basaltic grains containing plagioclase laths, clinopyroxene, and olivine aggregates in subophitic and intergranular textures. Colorless blocky glass fragments made up ∼5% of Lv grains.
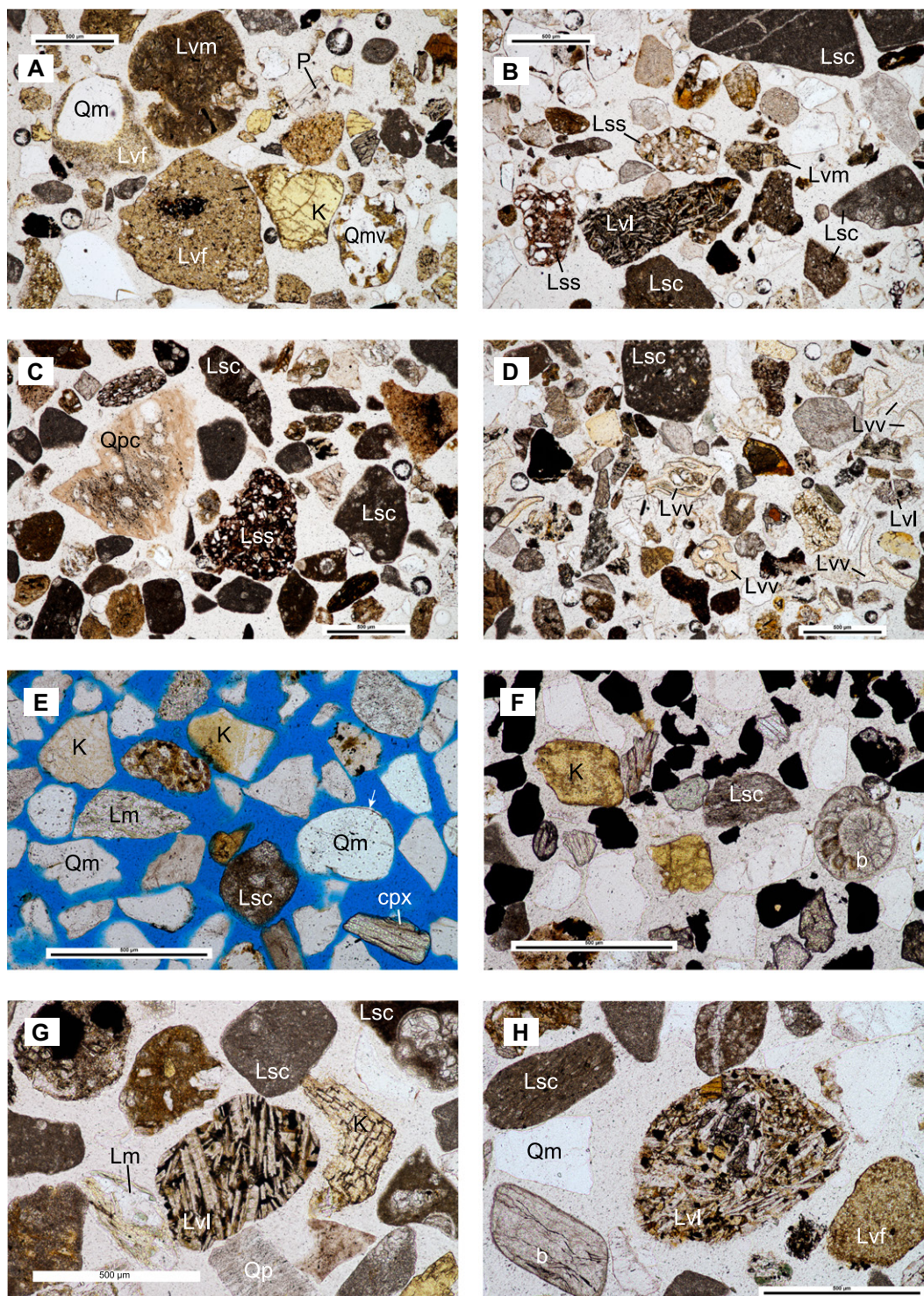
Figure 5. Photomicrographs of river and beach sands from eastern Mexico. All scale bars are 500 μm. (A) Volcanic-lithic sand of Río Tamuin (17EMX29). (B) Sedimentary and volcanic-lithic sand of Río Garces (17EMX16). (C) Río Vinazco (17EMX15). Colorless circular domains in chert grain (Qpc) are radiolaria. Lss grain is hematitic siltstone with angular Qm grains. (D) Río Tecolutla (17EMX05). Fragments of glass (Lvv) include blocky shards that preserve partial curvilinear vesicle walls, vesicular grains, and comb-like forms that resulted from flow elongation of vesicles. (E) Quartzose beach sand, Playa La Pesca, Tamaulipas (17NEMX07). (F) Beach sand, Playa Hermosa, Veracruz (17EMX28), with angular to rounded Qm, abundant opaque minerals, potassium feldspar, and foraminiferal bioclast (b). (G) Beach sand at Playa Nautla (17EMX02). (H) Beach sand at Santa Ana (17EMX1B) containing an unweathered basaltic grain with subophitic texture (Lvl) and an abraded bioclast (b). Abbreviations: cpx—clinopyroxene; K—potassium feldspar; Lm—metamorphic lithic grain; Lsc—detrital carbonate grain; Lss—siliciclastic sedimentary grain; Lvf—felsitic volcanic lithic grain; Lvm—microlitic volcanic lithic grain; P—plagioclase; Qm—monocrystalline quartz; Qmv—volcanic monocrystalline quartz with altered melt inclusions; Qp—polycrystalline quartz.

Litho-Quartzose and Quartzo-Lithic Sands of Eastern Mexico Beaches

Modern beach sands between the Rio Grande and central Veracruz are generally well sorted, fine to medium, and subrounded to rounded, although beaches in central Veracruz have grains that range from angular to subrounded. All beach samples contain bioclasts (1%–10%) represented by molluscan fragments, uncommon coralline fragments in more southern beaches, and well-preserved foraminiferal tests, which distinguish beach sands from river sands.

Beach sands had more QmFLt compositional variation than the entire set of fluvial samples. They consisted of litho-quartzose and quartzo-lithic sands with some more feldspathic samples (Figs. 4 and 5E). Some beach sands contained abundant opaque minerals, commonly in laminated placers (Fig. 5F). Average Qm (mean = 42%) was greater than that of other sand groups reported here and ranged as high as 76% at La Pesca, Tamaulipas (Table 4). LmLvLs grain proportions were less variable than those of river sand groups, with Lv grains ranging from 13%
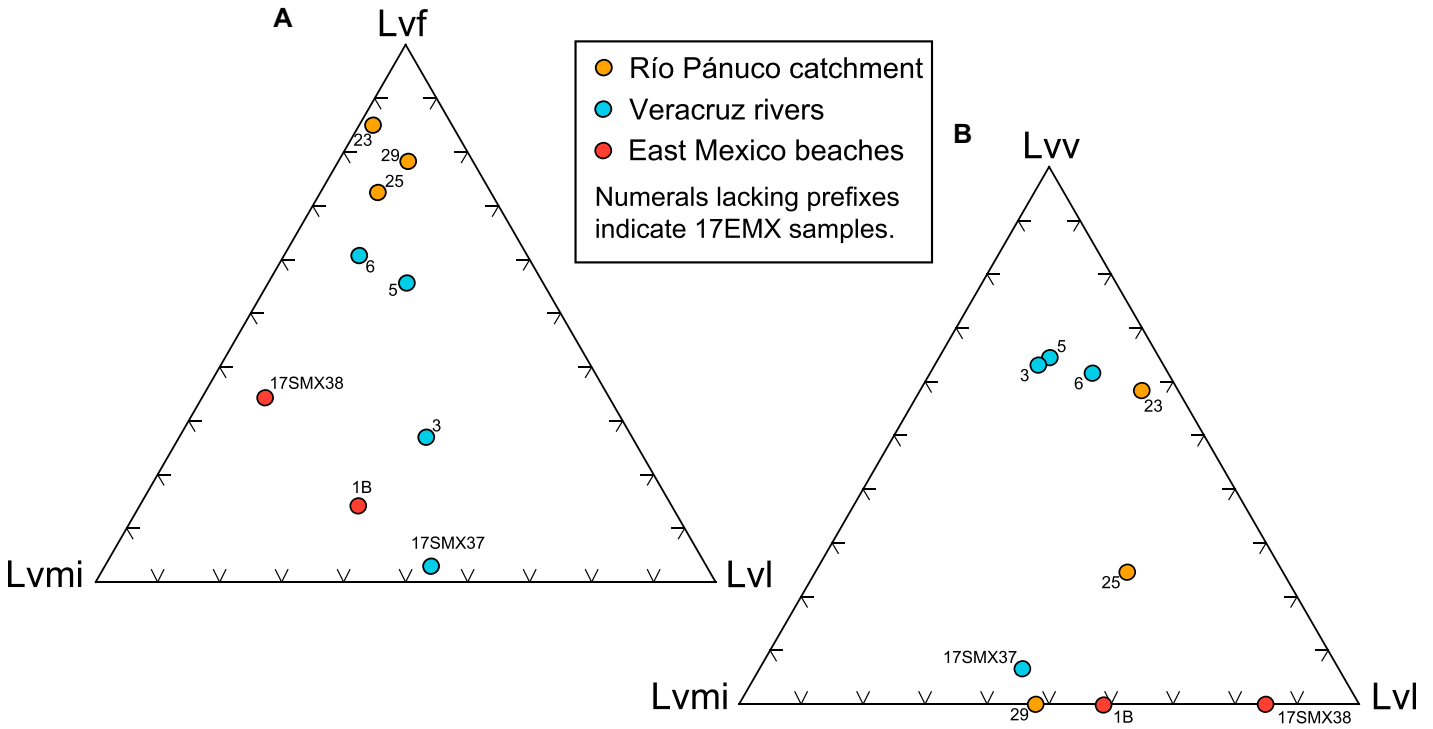
Figure 6. Volcanic lithic grain plots. (A). LvfLvmiLvl plot. (B) LvvLvmiLvl plot. See Tables 3 and 4 for grain definitions and plot symbols.

to 42%. Lvl grains in beach sand at Santa Ana (17EMX01B), midway between Playa Nautla and Playa Chachalacas, included beautifully preserved subophitic and intergranular textures consisting of plagioclase laths and small crystals of olivine in a glassy groundmass (Fig. 5H). A dune sand sample (Dunas Emilio Carranza, 17EMX01), located 3.5 km northwest of the beach at Santa Ana, had a quartzo-lithic composition ($Qm_{18}F_8Lt_{74}$) very similar to that of the sample at Playa Chachalacas (17SMX38; Fig. 4; Table 4). The dune sample contained 2% abraded bioclasts, indicating derivation from beach sediment, and it was strongly enriched in Ls grains (LmLvLs%Ls = 84%) by comparison with Playa Chachalacas (LmLvLs%Ls = 55%). Lsc grains dominated the Ls fraction at both localities: 92% of the dune sand Ls fraction consisted of rounded Lsc grains; similarly, 90% of the beach sand Ls fraction consisted of Lsc grains.

Beach sand composition varied systematically from north to south with distance from the mouth of the Rio Grande (Fig. 7). Monocrystalline quartz content (QmFLt%Qm) decreased from 79% at La Pesca, Tamaulipas, to 21% at Playa Chachalacas in central Veracruz, and Lt content increased from 8% to 70% over the same geographic interval. Volcanic lithic grain proportion of total modal framework grains (%Lv) displayed an irregular southward increase along the coast from lows of 4% and 3% at La Pesca (17NEMX07) and Playa Miramar (17EMX27) to a high of 30% at Playa

Chachalacas (17SMX38; Fig. 7; Table S1). The sample from Dunas Emilio Carranza lies near the longitudinal beach trends for both QtFL%Qt and QtFL%L, but its %Lv lies below the local trend of Veracruz beaches. Sand composition probably changes abruptly at river mouths, as previously noted in central Veracruz (Self, 1977). At the only place we were able to collect beach sands on both sides of a river mouth, at Río Pánuco, sand composition was quite different north and south

of the river at Playa Miramar (17EMX27) and Playa Hermosa (17EMX28). For example, Lsc grain content jumped from 5% to 24% of total grains and QmFLt%Qm decreased from 75% to 58% southward across the river mouth.

Detrital Zircon U-Pb Geochronology

As with our petrographically defined compositional suites, detrital zircon U-Pb ages of
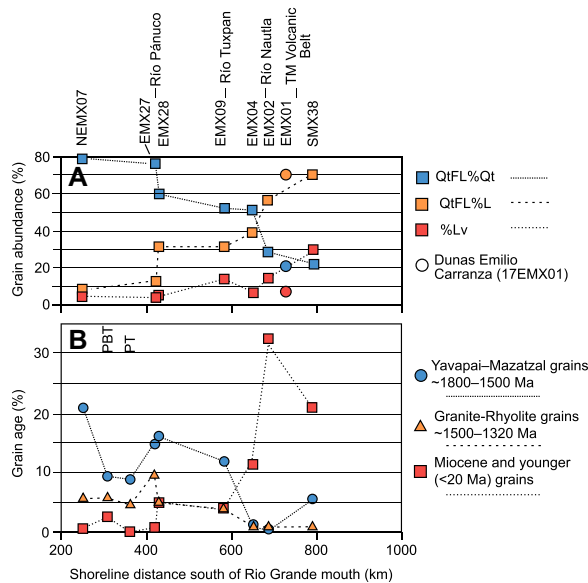
Figure 7. Compositional trends in eastern Mexico beaches. (A) Grain types. See Table 3 for grain definitions. %Lv—percent volcanic lithic grains (Lv) of total quartz-feldspar-lithics (QtFL) grain counts; other values are normalized percentages. TM—Trans-Mexican. (B) Detrital zircon age groups. See Table 2 for age group definitions.
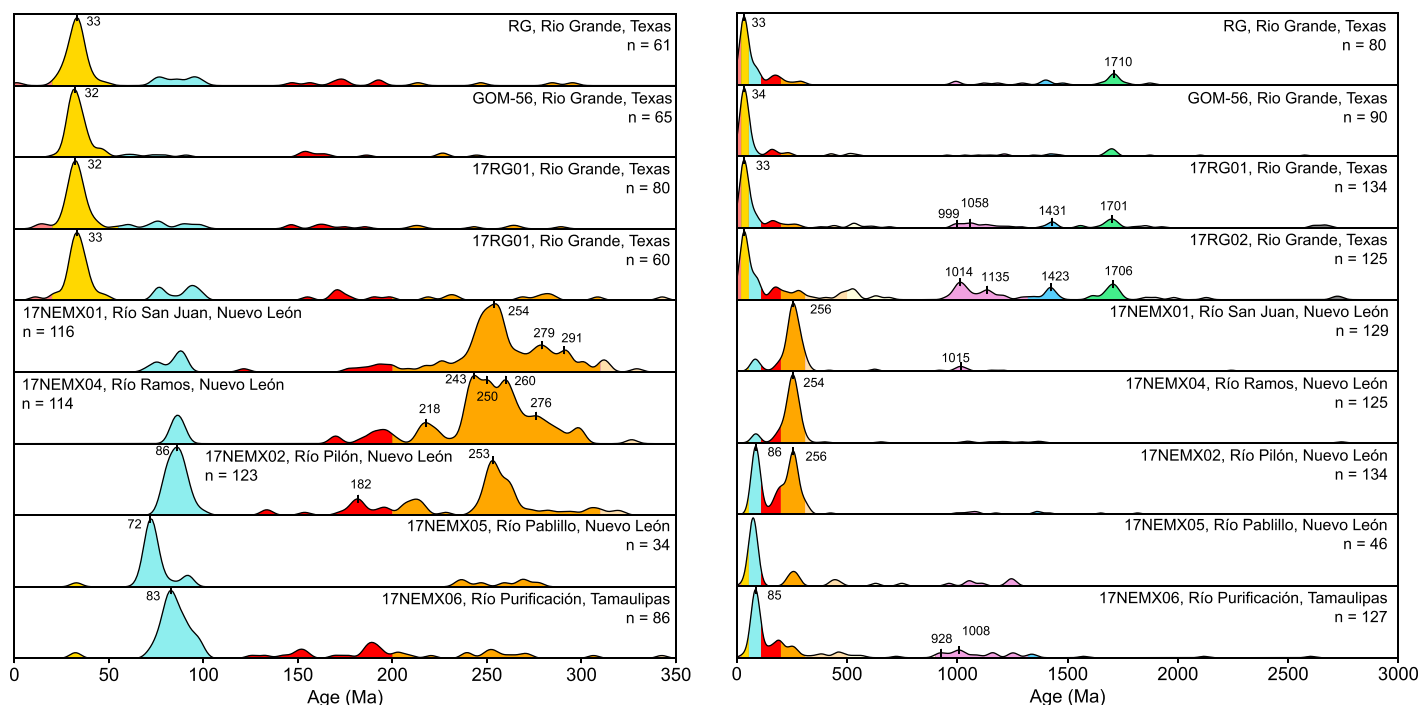
Figure 8. Kernel density estimator (KDE) plots of lower Rio Grande catchment. Ríos San Juan, Ramos, and Pilón drain to lower Rio Grande; Ríos Pablillo and Purificación drain to the Gulf of Mexico. Plots are arranged with distance downstream along the Rio Grande and southward in northeastern Mexico. Left plot: Grains 0–350 Ma. Right plot: Grains 0–3000 Ma. Grain age groups are explained in Table 2. Samples RG (abbreviated from Rio Grande) and GOM-56 are from Fan et al. (2019) and Blum et al. (2017). See Figure 2 for sample locations.

sand samples varied geographically and further delineated compositional characteristics and provenance of the sediment. The detrital zircon sample set is somewhat larger than the petrographic data set, with a combined Rio Grande and Nuevo León–Tamaulipas suite consisting of seven samples (Table 1), and a beach suite augmented by two published composite samples from Tamaulipas (PBT, PT; Ramos-Vázquez and Armstrong-Altrin, 2021). Zircon grains of the sample set ranged in age from 3184 Ma to 0.01 ka. Two negative grain ages were not included in the KDE plots. Percentages of different age groups are presented in Table S2. Samples from the various geographical regions are described according to their distinctive detrital zircon age distributions or chronofacies (e.g., Lawton et al., 2010; LaMaskin, 2012). Complete detrital zircon U-Pb data are provided in Table S3. In the following text, an age "population" refers to a complete sample of *n* analyses, with the population usually having a multimodal age "distribution" that consists of discrete "groups" of grain ages that overlap at 2σ error, with each age group having a modal age value, or "mode" (e.g., Saylor and Sundell, 2016).

Rio Grande Catchment

Samples from the Rio Grande and rivers draining into its lower course gave contrast-ing detrital zircon chronofacies. Sediment of the main river contained grains that range from Archean to ca. 1.3 Ma, with Proterozoic modes at ca. 1.7, 1.4, and 1.0 Ga (Fig. 8). Samples of lower river sand contained significantly more Grenville grains, defined as those zircon grains in the range 1320–900 Ma (Ectasian–Tonian), than the Laredo samples (11% and 19% compared to 6% and 7%; Table S2). All samples of Rio Grande sand had a dominant 55–20 Ma age group, which constituted 49% and 57% of grains from samples near Laredo and 39% and 26% of lower river samples, primarily in the age range ca. 37–27 Ma with a modal value at 32–33 Ma (early Oligocene). Samples from the rivers of Nuevo León and Tamaulipas lacked or contained few Proterozoic grains and were distinguished by a prominent late Permian age group with modes at ca. 256–254 Ma that made up 44%–76% of grains and a Late Cretaceous mode or modes in the range ca. 86–72 Ma that ranged from 7% to 34% of grains. Uncommon Jurassic–Early Cretaceous grains in the range 200–110 Ma (5%–11% of grains) were also present in most samples of northeastern Mexico rivers.

Catchments Draining Directly to the Northwestern Gulf of Mexico

Samples from the Ríos Pablillo and Purificación in Nuevo León and Tamaulipas were

distinctive in having single principal Late Cretaceous modes at ca. 72 Ma and 83 Ma (Fig. 8), which included 57% and 41% of grain ages, respectively. Both samples contained some Permian–Triassic grains (15% and 25%), and the Rio Purificación sample contained Grenville grains in the range 1320–900 Ma (18%) and some Jurassic–Early Cretaceous grains (13%), with the latter also present in the rivers draining to the lower Rio Grande.

Río Pánuco Catchment

Samples from the Río Pánuco catchment gave three different detrital zircon chronofacies, one represented by a single sample from the Río Tamuin, another by samples of the Ríos Moctezuma and Amajac, and a third by samples from the rivers that enter the Río Moctezuma via the Tempoal drainage (Fig. 9). Sample 17EMX29 from the Río Tamuin was unimodal at ca. 31 Ma, with 98% of grains in the age range 55–20 Ma (Table S2), and most of those ages (96%) in the range 34–28 Ma. Samples of the Moctezuma drainage (17EMX20–17EMX26) contained a variable percentage of Grenville grains that ranged from 1% to 32%. In a single sample (17EMX21) from the Río Amajac, a Paleocene mode was present at ca. 57 Ma, containing 13% of grain ages. Middle Eocene–late Oligocene and middle Miocene–Holocene age groups had
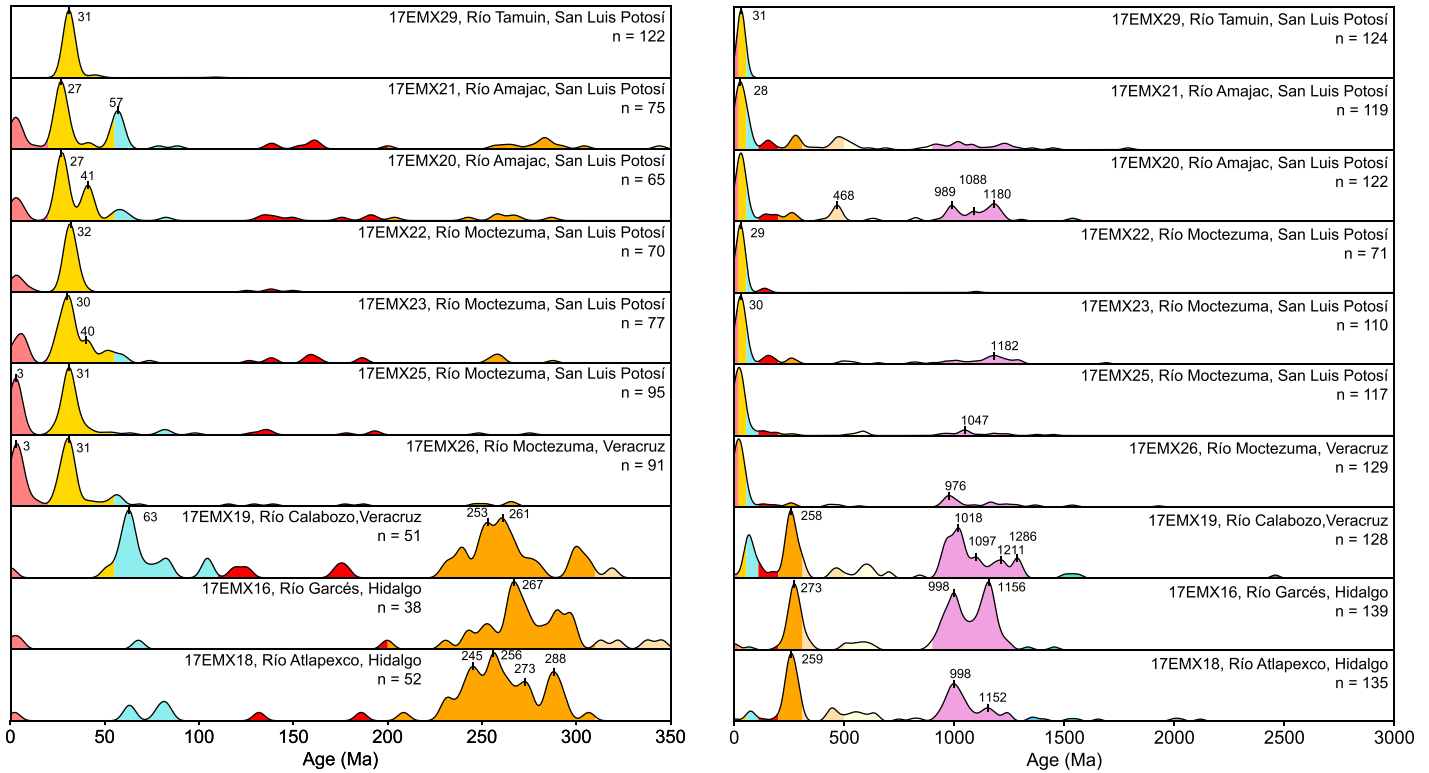
Figure 9. Kernel density estimator (KDE) plots of Río Pánuco catchment. Plots are arranged from north (top) to south across the drainage basin. Left plot: Grains 0–350 Ma. Right plot: Grains 0–3000 Ma. See Figure 2 for sample locations.

age modes at ca. 31–27 Ma and ca. 3 Ma in all samples of the Moctezuma drainage; these age groups constituted 36% and 18% of grain ages in the drainage. Samples from rivers draining into the Río Tempoal (17EMX16, 17EMX18, and 17EMX19) were distinctive in the catchment, having large percentages of Grenville grains (38%–65%) and late Carboniferous–Permian grains (22%–32%; Table S2). Grains in the range 110–55 Ma (mode ca. 63 Ma) formed 12% of a sample from the Río Calabozo. Cenozoic grains were uncommon in the three southern rivers of the Río Pánuco catchment.

Transverse Veracruz Rivers

Samples from the various Veracruz rivers had two distinctive detrital zircon chronofacies, a "Grenville-rich" chronofacies with dominant Grenville and late Pennsylvanian–Permian grains and a "Grenville-poor" chronofacies with fewer grains in those age groups (Fig. 10). Samples from the Ríos Vinazco, Pantepec, and Nautla had the Grenville-rich chronofacies, with age groups ca. 1320–900 Ma and 310–200 Ma averaging 29% and 30%, respectively. In contrast, samples from the Ríos Tecolutla and La Antigua were Grenville-poor, having averages of 11% and 3% for the same age groups (Table S2). All Veracruz samples had a prominent young

age group of 20–0 Ma that averaged 27% of all grain ages, with more abundant young grains in the Grenville-poor chronofacies samples (44%–90%) than in the Grenville-rich samples (4%–24%; Fig. 10; Table S2). The modal ages of the young age group were ca. 1 Ma in the Grenville-poor chronofacies, near ca. 3 Ma in the Grenville-rich chronofacies, and bimodal at ca. 13 and 3 Ma in the Río Nautla sample (17EMX03).

Beaches

Although the age distributions of beach samples were remarkably consistent in their Oligocene grain age proportions, other age groups varied markedly from north to south (Figs. 7B and 11). Grains of Proterozoic age groups 1800–1500 Ma and 1500–1320 Ma decreased proportionally southward from a high combined value of 24% at Playa La Pesca (17EMX07) to a low combined value of 1% at Playa Nautla (17EMX02) in Veracruz. An otherwise consistent decrease in the 1800–1500 Ma age group was interrupted by a dip in abundance to 9% at the beaches of southern Tamaulipas (samples PBT and PT; Ramos-Vázquez and Armstrong-Altrin, 2021) and an increase to 7% at the southernmost sampled beach, Playa Chachalacas, in Veracruz.

A southward decrease in proportion of the 1500–1320 Ma age group was interrupted by an increase to 9% directly north of the Pánuco river mouth. In the southernmost sample at Playa Chachalacas (17SMX38), the 1800–1500 Ma age group was represented by a range of younger ages from about 1600–1500 Ma that differed from the age range observed in northern beaches (Fig. 11). Grenville grains in the range 1320–900 Ma were present in all beach samples, doubling in abundance (22%–25%) in the two southernmost samples. Permian and Triassic grains were most abundant (15% and 25%) in samples from Veracruz beaches directly north of the Trans-Mexican volcanic belt (samples 17EMX02 and 17EMX04), and Jurassic and Cretaceous grains were abundant in beach samples from Tamaulipas and northern Veracruz, ranging as high as 34% at Playa Tesoro in southern Tamaulipas (Ramos-Vázquez and Armstrong-Altrin, 2021). Prominent in all beach samples except the one from Playa Nautla (17EMX02), Oligocene and Eocene grains constituted 18%–42% of individual samples and had consistent modal age values of 33–31 Ma. Young grains ranging ca. 20–0 Ma constituted 5% or less of grains in beach sands as far south as northern Veracruz and then increased southward beginning with
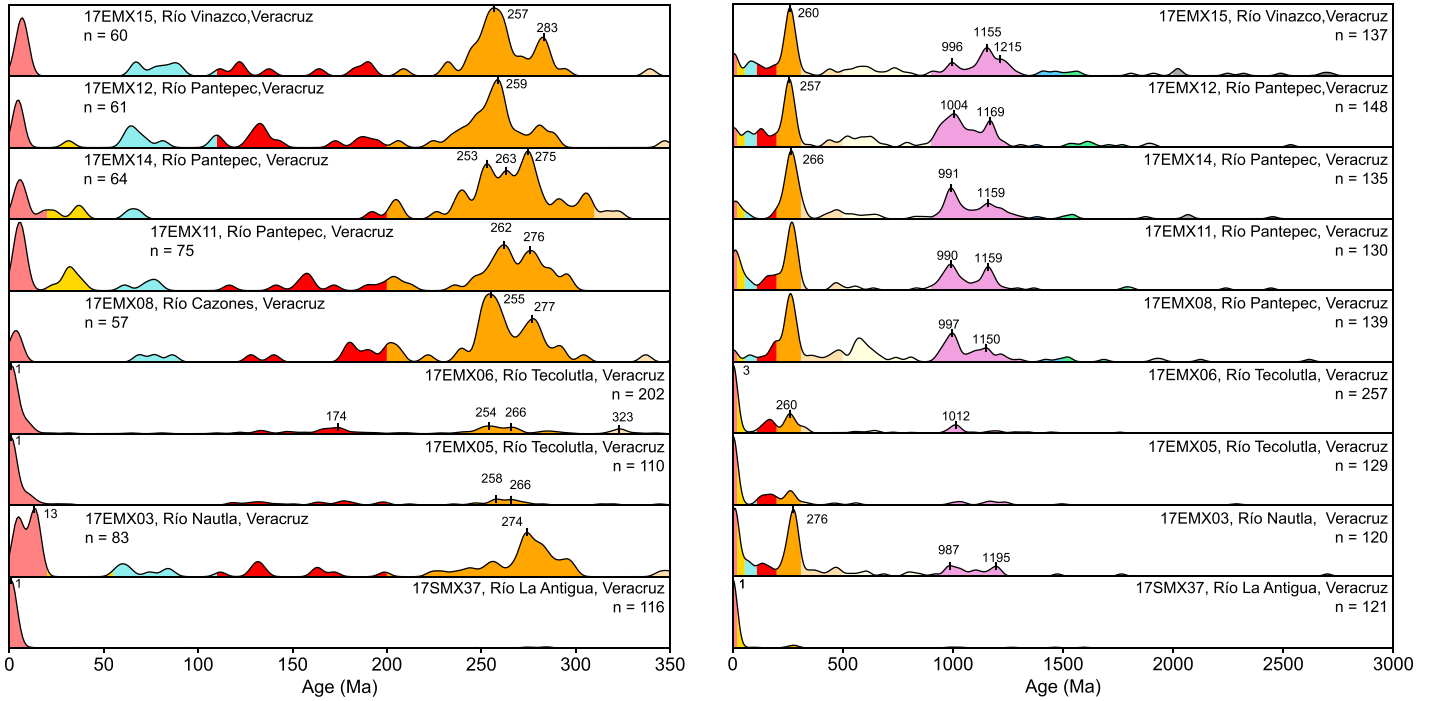
Figure 10. Kernel density estimator (KDE) plots of Veracruz transverse rivers. Plots are arranged from north (top) to south along the coastal plain. Left plot: Grains 0–350 Ma. Right plot: Grains 0–3000 Ma. See Figure 2 for sample locations.

the sample at Playa Tecolutla (17EMX04), achieving a maximum of 33% at Playa Nautla. This age group had a prominent mode at ca. 3 Ma in the sample from Playa Chachalacas.

Maximum Depositional Ages

Young grains that indicate the presence of active volcanism in a particular fluvial catchment are common in the zircon data set (Table 1).

Youngest single grains (YSG of Dickinson and Gehrels, 2009b) with ages less than 2 Ma were encountered most commonly in the Río Pánuco catchment, where 90% of the samples yielded

Figure 11. Kernel density estimator (KDE) plots of eastern Mexico beaches, arranged from north to south along coastline. Left plot: Grains 0–350 Ma. Right plot: Grains 0–3000 Ma. See Figure 2 for sample locations.

such ages, and 50% of samples had YSG ages younger than 200 ka (Table 1). The other sample, from the Río Tamuin (17EMX29), containing a high proportion of felsic volcanic lithic fragments, yielded a YSG of 28.3 ± 1.5 Ma and an equivalent multigrain MDA of 29.8 ± 0.2 Ma. About half of the Veracruz transverse rivers yielded YSG ages younger than 2 Ma, with one third of them having YSG ages younger than 100 ka. The YSG age in a Río Tecolutla sample (17EMX05) was −0.07 ± 0.12 Ma; the second youngest grain was 0.093 ± 0.042 Ma (Table 1). Beach sands typically yielded older YSG ages, although six samples yielded YSG ages younger than 2 Ma, and two samples yielded YSG ages younger than 2 ka.

Statistical Comparison of Samples

A multidimensional scaling plot (Vermeesch, 2013; Saylor and Sundell, 2016) illustrates the statistical dissimilarity of the age distributions of all samples collected as part of this study (Fig. 12). Rio Grande and beach samples exhibit high grain-age correspondence, with northern beaches and the two lower river samples forming a group having comparable sample variability among the river samples and beach samples, particularly those from Tamaulipas and northern Veracruz beaches. Rio Grande

samples from Laredo plot near one another but have less affinity with downstream and beach samples. Nuevo León samples from rivers draining to the Rio Grande (NEMX01, NEMX02, NEMX04) form a group that is distinct from all other samples, but with some affinity to the Río Pablillo and Purificación samples (17NEMX05 and 17NEMX06), also derived from the Sierra Madre Oriental and somewhat dissimilar to one another. Samples from the Río Pánuco catchment display extreme variability, with samples from the Río Moctezuma (17EMX22, 17EMX23, 17EMX25, and 17EMX26) and Río Amajac (17EMX20 and 17EMX 21) distributed on the diagram generally in order of their positions along the river courses. The most upstream Río Moctezuma sample (17EMX22), above the river's confluence with the Río Amajac, is dissimilar to the other samples of the Ríos Amajac-Moctezuma group. Moctezuma samples downstream of the confluence, interpreted as predam sediment (17EMX23 and 17EMX26), are not decidedly dissimilar compared to a postdam sample (17EMX25). Tributaries of the Río Tempoal watershed (17EMX16, 17EMX18,

17EMX19) form a distinct group dissimilar to the Río Moctezuma samples and instead have higher correspondence with Veracruz samples. The sample from the Río Tamuin (17EMX29) is the most compositionally distinct sample of the Pánuco catchment. Veracruz river samples form a band of points arranged roughly geographically from north to south, with the southernmost Río La Antigua sample (17SMX37) representing a marked outlier.

Core-Rim Age Pairs

A plot of paired core-rim ages produced by depth profiling of individual zircon grains revealed that concordant detrital zircon age pairs ($n = 101$, with individual samples yielding from 0 to 12 age pairs) occupy two distinct data clusters defined by numerous age pairs: a less distinct cluster of young core ages, and dispersed analyses that probably resulted from insufficient data to generate obvious groupings (Fig. 13). Distinct clusters include overlapping rim ages in the range 1050–920 Ma with core ages ranging 1320–1090 Ma and 1400–1500 Ma (clusters 1 and 2, respectively), and a

Figure 12. Two-dimensional multidimensional scaling (MDS) plot for detrital-zircon U-Pb age distributions of modern river and beach sand adjacent to western Gulf of Mexico. Axis scales are calculated dissimilarity values (Vermeesch, 2013). Samples that plot closer together have detrital zircon age distributions with greater correspondence, or less dissimilarity, than samples with more scatter. The MDS plot was constructed using detritalPy (Sharman et al., 2018). Data points lacking letter prefixes are 17EMX samples.

Figure 13. Plot of corresponding core and rim ages from individual zircon grains. Labeled clusters are discussed in text.

point swarm of lower data density consisting of Grenville–Neoproterozoic cores (1230–830 Ma) and Neoproterozoic–late Paleozoic rims in the ranges 660–400 Ma (cluster 3) and 350–250 Ma (cluster 4). The 50 m.y. interval between clusters 3 and 4 contains only two grains. A fifth, more dispersed, cluster of age pairs consists of young rim ages ranging ca. 110–0.5 Ma with core ages that range from ca. 437 to 36 Ma (cluster 5). The remainder of the plot contains widely dispersed age pairs, some of which are described separately.

Clusters 1 and 2, with Mesoproterozoic to Grenville cores and either Grenville rims or pre-Grenville rims, are occupied by analyses from rivers of the Pánuco drainage basin and transverse rivers of Veracruz, as well as beach samples from central Tamaulipas to central Veracruz. Cluster 3 is represented by samples from the same drainage basins and beaches as clusters 1 and 2, whereas cluster 4 is dominated by Veracruz drainages and contains a single grain from the Río Garces of Nuevo León (17EMX16). Cluster 5 contains three analyses with Paleogene rims from a Rio Grande sample (17RG01), two analyses with Pleistocene rims on Mesozoic cores from the Río Tecolutla (17EMX06; 1.9 and 110 Ma) and Río La Antigua of Veracruz (17SMX37; 0.5 and 246 Ma), and an Eocene rim on a Jurassic core from Playa Miramar in Tamaulipas (17EMX27; 47 and 189 Ma).

Individual grain ages of interest are present in several samples. Sample 17NEMX07 from Playa La Pesca in Tamaulipas has two old age pairs (1.675, 1.414 Ga and 1.485, 1.049 Ga).

Sample 17EMX27 from Playa Miramar has a grain with a core-rim pair of 1692 and 432 Ma. Playa Hermosa (17EMX28) yielded a Mesoproterozoic core with an Oligocene rim (1568 and 28 Ma). Neoproterozoic and Paleozoic cores with Paleozoic and Mesozoic rims were recovered from samples of the Pánuco drainage basin ($n = 2$), Veracruz drainages ($n = 4$), and the Ríos Purificación and San Juan ($n = 1$ each). Zircon cores ranging 1.65 to 1.35 Ga having Paleozoic to Jurassic rims were encountered in samples of Nuevo León rivers and the Rio Grande ($n = 4$), and in single grains from a sample of the Río Amajac (17EMX21) and the Río Pantepec in Veracruz (17EMX11).

DISCUSSION

An understanding of possible sediment sources in coastal eastern Mexico derived from analysis of sand composition provides important quantitative insight into sediment transport along the western side of the Gulf of Mexico. Moreover, the integrated petrographic and U-Pb detrital zircon provenance approach presented here can be applied to evaluation of sediment budgets in linked sediment-transport systems elsewhere in the world. Unexpected changes in beach sand composition along a longshore transport path can inform prediction and investigation of coastal reaches that might be subject to net erosion and sediment recycling. Alongshore decreases in specific grain age modes can signal potential sites of sand deposition or loss of sand from the shelf to the deep basin, both of which

have implications for long-term beach viability or sediment resource potential.

Seasonal Surface Currents in Western Gulf of Mexico

The net transport direction of sand by littoral currents (e.g., Bascomb, 1980) is not predicted a priori by longshore surface currents of the western Gulf of Mexico on the Tamaulipas-Veracruz shelf, which are seasonally opposed (Fig. 14; Zavala-Hidalgo et al., 2003). Coastline-parallel surface currents that attain a mean monthly velocity of 0.70 m/s are northward from May to August and southward from September to March. The north-directed spring and summer current encounters opposing confluent flow on the Texas coast north of the Rio Grande near Corpus Christi (Fig. 14A), whereas south-directed winter surface flow encounters a strong southwest-directed countercurrent at the Bay of Campeche in the southernmost part of the Gulf of Mexico near the Veracruz-Tabasco state line (Fig. 14B). Self (1977) inferred net annual northward transport of beach sand in central Veracruz on the basis of prograding sand spits and river-mouth bars but noted that winter longshore transport moved sand as much as 60 km south of the Tecolutla and Nautla river mouths. In addition, abrupt changes in mineral percentages of sand at beaches near river mouths were inferred to indicate a fluvial origin for beach sand by rivers draining the Sierra Madre Oriental (Self, 1977). Variation of sediment composition along the coast thus can provide critical additional insight
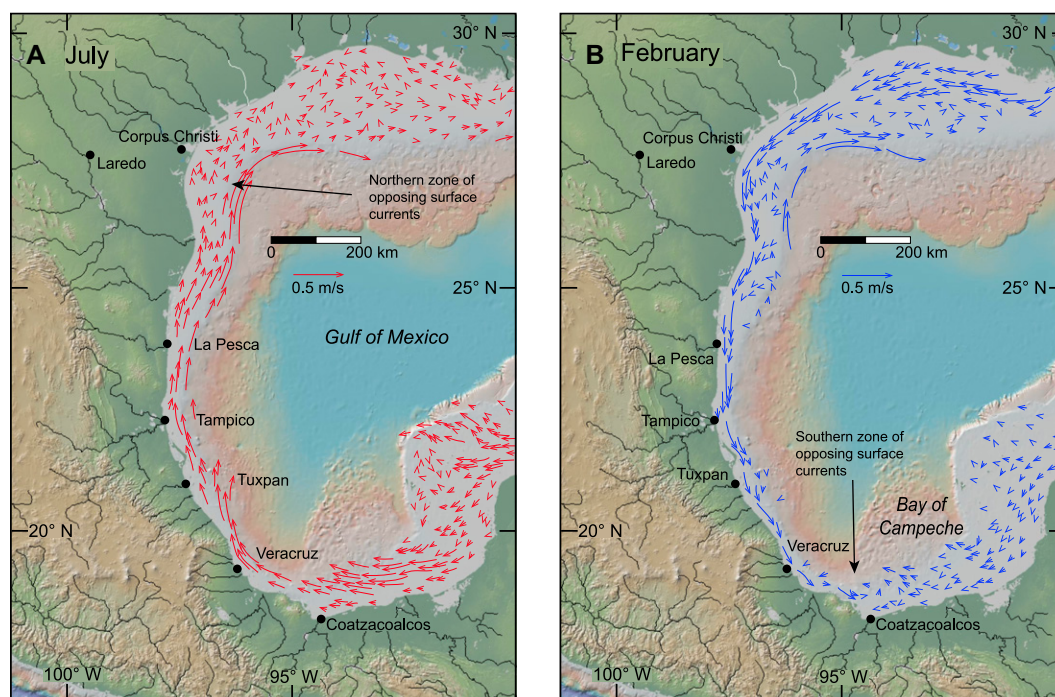
Figure 14. Seasonal surface currents on the western, northern, and southern shelves of the Gulf of Mexico, generalized and redrawn on GeoMap base after Zavala-Hidalgo et al. (2003). (A) Summer currents. (B) Winter currents.

into long-term net sediment transport direction as well as discrete locations of sediment input to littoral transport.

Sources of Detrital Modes and Detrital Zircon Age Groups

Sand compositions and detrital zircon age distributions along the east coast of Mexico indicate not only important sediment contributions from northeastern Mexico, but also from the western United States, specifically the Rocky Mountain region, where Paleoproterozoic basement rocks are exposed in southern Colorado and northern New Mexico in the headwaters of the Rio Grande and Pecos River (Fig. 1), as much as 3650 km from the beaches of central Veracruz. In the drainage headwaters, igneous and metamorphic rocks of the Yavapai-Mazatzal and Granite-Rhyolite basement provinces and widespread Upper Paleozoic sedimentary rocks derived from them are inferred to give rise to important age groups of zircon grains in the ranges 1800–1500 Ma and 1500–1320 Ma, respectively (Table 2; e.g., Whitmeyer and Karlstrom, 2007; Gehrels et al., 2011; Leary et al., 2020). These basement ages are not present in Mexico except locally in Sonora (e.g., Iriondo et al., 2004; Anderson and Silver, 2005). Therefore, the combination of these two Proterozoic age groups in Rio Grande sediment and beaches of Tamaulipas and northern Veracruz indicates ultimate basement sources lying north of Mexico.

Zircon ages in the range 1320–950 Ma, which do not have a widespread distribution in basement rocks of the Rocky Mountains and thus indicate a more ambiguous origin of the sands in this study, are generally called "Grenville." Outcrops of Grenville basement are locally present along the course of the Rio Grande at El Paso in far west Texas, but, more importantly, Grenville grains dominate eolian Permian and Jurassic strata that crop out widely in the Colorado Plateau and southern Rocky Mountains (Dickinson and Gehrels, 2003, 2009a) and are drained by headwater tributaries of the Rio Grande (Fig. 1). Grenville basement and strata composed of grains derived from that basement also crop in the Huizachal and Huayacocotla uplifts of the Sierra Madre Oriental, which are drained by rivers of the Pánuco catchment and Veracruz transverse rivers; therefore, local Mexican sources, as well as the Rio Grande catchment, can generate abundant Grenville zircon ages.

Locally derived grain age groups of the study area yield important perspective on possible sediment inputs to the coastal littoral transport system. Late Paleozoic and Mesozoic zircon grains, common in sediment of rivers draining via the San Juan catchment into the lower Rio Grande

(Fig. 2; samples 17NEMX02, 17NEMX04, 17NEMX01) and directly to the Gulf of Mexico (samples 17NEMX05, 17NEMX06), were eroded from deformed Mesozoic strata of the Sierra Madre Oriental fold-and-thrust belt (Figs. 1 and 2). These grain ages are uncommon in sediment of our Rio Grande samples collected downstream of the San Juan confluence and in published samples of Rio Grande sediment from upstream of the confluence (Blum et al., 2017; Fan et al., 2019). In contrast, Moore et al. (2021) reported more abundant late Paleozoic, Jurassic, and Early Cretaceous grain ages in a sediment sample from the lower river, attributing observed age distributions to reworking of Cenozoic coastal plain strata that resulted from the construction of dams on the Río San Juan and lower course of the Rio Grande. We also note a significant increase in Grenville grains in lower river samples, which also is likely a result of recycling of coastal plain strata. Although petrographic data from rivers draining the northern part of the Sierra Madre Oriental are limited, a single sample of the Río Purificación (17NEMX06) indicates dominance of sedimentary lithic detritus and tuff grains derived from Cretaceous strata and feldspar-bearing siltstone grains derived principally from Jurassic siliciclastic strata such as the Galeana Sandstone, large clasts of which are present at the site of sample 14NEMX04 on the Río Ramos. Carbonate strata do not typically yield sand-sized detrital zircon grains; therefore, the principal age mode at ca. 83 Ma (Fig. 8) in this sample indicates recycling of ash-rich Upper Cretaceous shale and sandstone intercalated with the carbonate rocks (e.g., Velasco-Tapia et al., 2016; Juárez-Arriaga et al., 2019a). Abundant Cretaceous and Jurassic grains, as well as lesser Permian and Triassic grains, in the beaches of Tamaulipas imply that sand eroded from Mesozoic strata of the Sierra Madre Oriental and transported to the lower Rio Grande and directly to the Tamaulipas coast was an important pre-dam component of sediment reaching beach and coastal plain settings.

Oligocene zircon grains within the age group 55–20 Ma represent an almost universal component of sediment in the Rio Grande (26%–39% of all grains), the northern rivers of the Río Pánuco catchment (27%–98% of all grains), and the beaches of eastern Mexico north of the Trans-Mexican volcanic belt (23%–42%; Figs. 8, 9, and 11; Table S3). These grains are typically, although not always, associated with sands having high Lv contents. Sands with high Lvf proportions (e.g., Río Moctezuma samples 17EMX23 and 17EMX25) commonly have abundant grains in this age group (41%; Fig. 6; Table S3); notably, sample 17EMX29 from the Río Tamuin (with LvfLvmiLvl%Lvf = 79%)

contains almost exclusively Oligocene grains (98%; Table S3). These Oligocene grains, derived from extensive silicic volcanic fields of northern Mexico and the southwestern United States, have several possible geographic sources, including the Trans-Pecos volcanic field of west Texas and northernmost Chihuahua, the high plateau region of the Sierra Madre Occidental in western Mexico, and the southeastern extent of that volcanic field in San Luis Potosí. The grains in the Rio Grande samples could have been derived directly from the Trans-Pecos volcanic field, with a restricted age range of ca. 33–32 Ma (Cepeda and Henry, 1983), or transported from the more distant Sierra Madre Occidental volcanic field in Chihuahua by the Río Conchos (Fig. 1). More distant contemporary volcanic fields such as the San Juan volcanic field in southern Colorado, lying in the headwaters of the Rio Grande, and parts of the Mogollon-Datil volcanic field in west-central New Mexico may also have contributed grains in the age range ca. 36–26 Ma (Table 2; Lipman and McIntosh, 2008; Chapin, 2012). Felsitic volcanic lithic grains of the Río Tamuin and accompanying Oligocene zircon grains having a more restricted age range (ca. 34–28 Ma) than the zircon grains of the Rio Grande (ca. 36–26 Ma) can be confidently traced to the southeastern part of the Sierra Madre Occidental volcanic field in the headwaters of the Río Tamuin (Table 2).

A single young grain with an age of 1.3 ± 0.1 Ma reported from a Rio Grande sand sample (Fan et al., 2019) was probably ultimately derived from the Jemez Mountains volcanic field in northern New Mexico, where voluminous rhyolite tuffs were emplaced during caldera collapse in the range 1.6–1.2 Ma ($^{40}Ar/^{39}Ar$ ages; Table 2; Spell et al., 1996; Goff and Gardner, 2004; Nasholds and Zimmerer, 2022). An alternative possible source for this grain age is recycling of pumice beds derived from the Jemez eruptions and transported downstream by the ancestral Rio Grande to be deposited in the Pleistocene Camp Rice Formation of the southern Rio Grande rift in New Mexico (Mack et al., 1996) prior to the river's integration with the modern lower stream course. Pleistocene grains were not detected in our Rio Grande samples and are evidently not abundant in modern river sediment downstream of New Mexico; nevertheless, these Pleistocene grains represent potentially important tracers of sediment derived from the upper Rio Grande.

Sources of Rio Grande sediment that have caused a lack of age correspondence between lower river samples and those from Laredo remain an unresolved problem due mainly to insufficient numbers and geographic distribution of samples. Notably, grains in the age ranges 1500–1320 Ma and 1320–900 Ma

increase downstream from 5% and 6% of all grain ages from a modern sand sample at Laredo (Fan et al., 2019) to a mean of 10% and 21% near the river mouth (our samples 17RG01 and 17RG 02). Grains in the age range 55–20 Ma decrease from 49% at Laredo to a mean value of 33% in our samples. Statistical comparison of a sample of modern channel sand collected near Brownsville, Texas, and downstream of the Río San Juan confluence with published age distributions of coastal plain strata of Texas led Moore et al. (2021) to infer that their downstream sample was sourced primarily from erosion of Oligocene strata following dam construction. An alternative possible source for lower river sediment lies in Upper Cretaceous–Paleogene strata lying north of the Sierra Madre Oriental in Mexico. These strata are incised by ephemeral stream courses that join the Río San Juan downstream of our samples in the catchment (Fig. 2), and they contain Proterozoic age peaks near 1.7, 1.4, and 1.1 Ga (Lawton et al., 2009), similar to those in our lower river samples, as well as Early Cretaceous and Jurassic grains present in the samples of the lower river (Moore et al., 2021) but uncommon in our lower river samples. Additional sampling of the lower Rio Grande and the lower reach of the Río San Juan is needed to provide improved insight into this problem. Although pertinent to anthropogenic alteration of Rio Grande sediment budgets, the proximal sources of these Proterozoic and Mesozoic grains do not alter our inferences, outlined below, about the relationship of Rio Grande sediment to that of northeastern Mexican beaches.

Sediments entering the Río Pánuco main stem via the Río Tempoal share distinctive compositional characteristics and detrital zircon chronofacies with the transverse rivers of northern Veracruz. They contain low quantities of potassium feldspar (Fig. 4D) and abundant Permian–Triassic and Grenville grains (Figs. 9 and 10), an age combination not common to other river sediment of the study area. Although Permian–Triassic grains are common in some river sediment of Nuevo León, Grenville grains are rare in sediment of those rivers. In Veracruz, Grenville grains were derived from deep canyons of the Sierra Madre Oriental that give rivers access to a geographically restricted assemblage of metamorphic basement rocks, overlying Permian volcanic and volcaniclastic strata, and Jurassic strata in the Huayacocotla uplift (Fig. 2; e.g., Suter, 1990). Sediment of Veracruz transverse rivers also contains a higher proportion of Neogene and younger grains and volcanic-lithic fragments than that of the Río Tempoal tributaries (Figs. 4C, 9, and 10), indicating an increased contribution of sediment from post-Oligocene volcanic rocks. Pyroxene grains and lathwork

volcanic lithic fragments (Lvl) appear abruptly at Playa Nautla (17EMX02; Fig. 5G), signaling an important mafic volcanic sediment source in the nearby Eastern Alkaline volcanic province of the Trans-Mexican volcanic belt. In the southernmost fluvial samples from Veracruz, with the exception of the Río Nautla, the proportions of Grenville and Permian–Triassic grains diminish where upper reaches of the southern rivers do not encounter the Huayacocotla uplift.

Detrital Zircon Core-Rim Ages

Core-rim age pairs of detrital zircon grains in this study (Fig. 13) provide additional information on details of sand provenance. Many age pairs in ancient strata of North America are nondiagnostic regarding provenance (e.g., Liu et al., 2022), but their presence in grains of modern depositional systems, particularly rivers, precludes possible source regions that lie outside of a particular watershed or down-transport from a particular sample site. A couple of age pairs deserve mention. A grain from the Playa La Pesca sample (17NEMX07) in cluster 1 consisting of both Grenville cores and rims could have come from the Appalachian orogen via recycling of Permian or Jurassic eolianite strata of the Colorado Plateau (e.g., Dickinson and Gehrels, 2009a), rather than from basement of the Sierra Madre Oriental because the beach lies up-transport from the Mexican basement sources. Perhaps the most definitive core-rim pair in the data set is a single grain from Playa La Pesca (17NEMX07) that consists of a 1.7 Ga core with a 1.4 Ga rim, representing a grain that originated in Yavapai basement and was incorporated into a Granite-Rhyolite intrusion. This is typical of Rocky Mountain provenance (e.g., Gehrels et al., 2011) and corroborates the modal grain-age distribution of the sample. Nevertheless, recycling from a Mesozoic sandstone ultimately derived from a southwestern U.S. source, for example, in the Sierra Madre foreland (e.g., Lawton et al., 2009), is not precluded.

Interpretation of age-pair grain clusters generally corroborates inferences drawn from the KDE plots. Grenville core-rim pairs of cluster 1 encountered principally in rivers of Veracruz and the Río Pánuco catchment likely represent local Mexican sources, principally Grenville basement and Permian and Jurassic strata derived from that basement in the Huizachal and Huayacocotla uplifts (Fig. 1). Older grain cores of cluster 2, also with Grenville rims and from the Río Pánuco and Veracruz river catchments and Veracruz beach sample, are more difficult to pinpoint as to source. Their presence in local Mexican rivers suggests a source consisting of old Amazonian grains incorporated in Grenville

crust (e.g., Cardona et al., 2010). Grains of clusters 3 and 4, with Grenville and Neoproterozoic cores and Neoproterozoic and early Paleozoic cores, respectively, can be attributed to local Mexican sources in the Sierra Madre Oriental. Cluster 5, consisting of Phanerozoic cores with Cretaceous to recent rims, represents sources characterized by inheritance of xenocrystic cores by Mesozoic and Cenozoic to recent magmatic systems. Cretaceous rims were probably created by magmas of the Cordilleran arc on the western margin of Mexico that incorporated older grains. Oligocene rims are mainly encountered in grains of Rio Grande sediment (17RG01), where one grain with an approximately contemporary core may represent an antecryst from a long-lived magma chamber such as those which have been described from the Sierra Madre Occidental volcanic field (Bryan et al., 2008). Mesozoic and Paleozoic cores likely represent inheritance of sedimentary grains by Oligocene magmas.

Our core-rim data suggest limited inheritance of older zircon grains by young magmas of the Trans-Mexican volcanic belt. Rims in the age range 20–0 Ma, both Pleistocene, are present in only two older cores, one Early Triassic and one Early Cretaceous. This represents only 2% of our total set of grains with core and rim ages. This is in notable contrast to xenocrystic cores of zircon grains collected from La Malinche stratovolcano in the eastern Trans-Mexican volcanic belt (Fig. 2), which yielded 12% xenocrystic cores, most commonly Early Cretaceous and Eocene–Oligocene (Gómez-Tuena et al., 2018). This apparent disparity probably resulted from our random encounters of core-rim ages on individual grains during depth profiling, as opposed to a deliberate search for xenocrystic cores using cathodoluminescence imaging by Gómez-Tuena et al. (2018). Nevertheless, the grain with an Early Cretaceous core and Pleistocene rim in our Río Tecolutla sample (17EMX05) strongly suggests a source at La Malinche in the river's headwaters.

Maximum Depositional Ages of Modern Sediment

The new data presented here from modern Mexican sands significantly expand the database of modern sands derived from active volcanic settings and indicate that active volcanism can be detected from YSG ages in both rivers and beaches. MDAs of beach and river samples tend to decrease southward along the Mexican coastal plain as river catchments extend into the Miocene–recent Trans-Mexican volcanic belt. Sands of rivers having catchments that reach stratovolcanoes of the Trans-Mexican volcanic belt consistently contain YSG ages younger

than 200 ka, with uncertainties that cause the ages to approach 0 Ma (Table 1). Calculations of MDA from multiple grains tend to yield older ages than estimates from YSG ages. As noted in a recent compilation of U-Pb detrital zircon ages from modern and Holocene samples, methods for determining MDA that rely on one or two young grain analyses are more likely to yield MDA values younger than the true depositional age than methods that employ larger numbers of grains (Sharman and Malkowski, 2020). In

the present study, only one of 11 samples having young grain ages (younger than 200 ka) yielded a negative grain age (Table 1). Therefore, although we recognize the MDA uncertainty associated with single grain methods, particularly in ancient rocks (e.g., Dickinson and Gehrels, 2009b), the YSG ages obtained from our sample set of modern sand in eastern Mexico, which includes an active volcanic province, provide more reliable MDA estimates than multigrain methods.

Geographic Trends in Sediment Composition

Key north-south variations in detrital zircon content of beach sands reveal a steady southward diminution in the proportion of sand grains that can confidently be attributed to sources north of Mexico (Fig. 15). Yavapai and Mazatzal grains in the age range 1800–1500 Ma and Granite-Rhyolite grains near ca. 1400 Ma decrease proportionately southward, finally having abundances
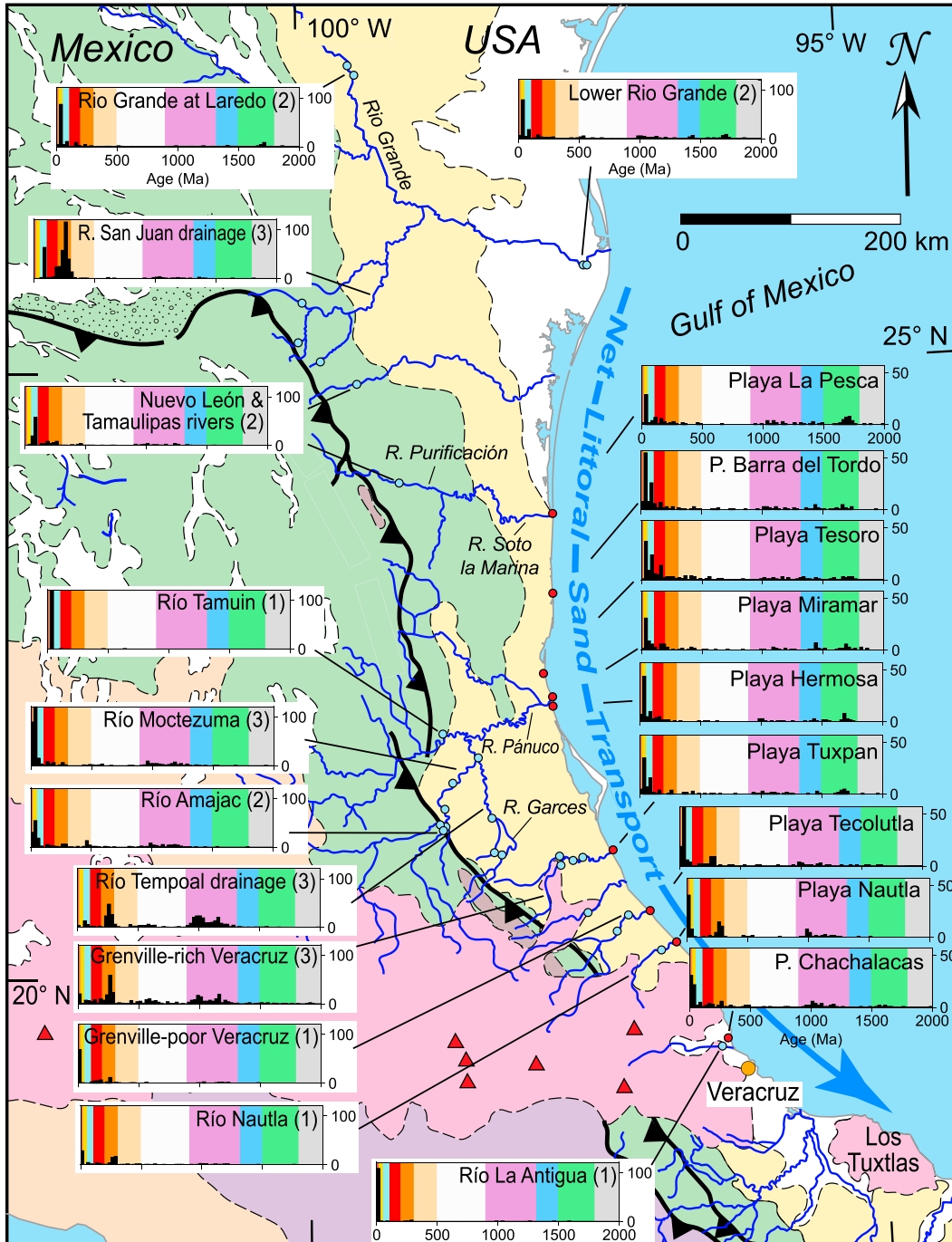
Figure 15. Normalized histograms of U-Pb zircon age distributions for combined samples from river catchments and individual beach sand samples along the west coast of the Gulf of Mexico. Blue arrow indicates inferred net coastal sand transport by longshore currents. Locations of principal sand transport to deep Gulf of Mexico remain unknown, but one may lie near Sierra de Los Tuxtlas (e.g., Hessler et al., 2018). Histogram bin width = 25 m.y. Beach and river samples were normalized at different scales to permit combining (*n*) samples in river sands. Subsets of representative Grenville-rich and Grenville-poor Veracruz river samples were selected to permit the normalized scale for histograms. Color bands indicate age groups illustrated in kernel density estimator (KDE) plots of Figures 8–11.

of less than 1% at Playa Nautla. The apparent disappearance of the old grains there is in part a function of sample size, because samples with $n < 117$ may not record grain-age groups that make up less than 5% of the sample population (Vermeesch, 2004). Therefore, with present sample sizes, we can only infer that zircon grain proportions derived from sources north of Mexico drop to less than 5% of zircon in the beach sand or that these ages reside in zircon grains smaller than those we analyzed. Another factor may be that south-directed littoral transport encountered a region of more strongly north-directed seasonal transport along the coast of central Veracruz (e.g., Self, 1977). Systematic sampling of beach sands near river mouths during the distinct periods of north- and south-directed surface currents might serve to define seasonal variation in sediment transport more precisely. The Proterozoic grains with a different age distribution in the range 1800–1500 Ma at Playa Chachalacas (17SMX38) likely derive from recycling of Triassic–Jurassic strata containing grains of this age, ultimately having an Amazonian source, in the southern part of the Sierra Madre Oriental fold-and-thrust belt (e.g., Molina Garza et al., 2020). Jurassic and Cretaceous grains, which are common in the northern river and beach samples, likewise diminish southward to constitute only 3% of the sample at Playa Nautla. Conversely, post–20 Ma zircon grains attributable to a Trans-Mexican volcanic belt source are rare to absent in beaches north of the Pánuco river mouth, the northernmost sampled catchment to tap into the Trans-Mexican volcanic belt. Two grains near 1.2 Ma are present in a sample from Playa Barra del Tordo in Tamaulipas, and thus could have been delivered northward along the coast; however, a pyroclastic origin or a source in the Jemez Mountains volcanic field in the upper reaches of the Rio Grande is equally plausible. Similarly, Moore et al. (2021) inferred a lack of northward transport of Trans-Mexican volcanic belt–sourced grains from southeastern Veracruz on the basis of their absence in sands of the Rio Grande delta.

Two aspects of the sand composition and detrital zircon age distribution data set indicate that, in addition to being derived from sources north of Mexico, some beach sediment of northeastern Mexico is presently being recycled from the Holocene coastal plain. For one thing, the proportion of Proterozoic grain ages in Tamaulipas beach sands consistently exceeds that of the modern Rio Grande and increases southward through the state (Figs. 7B, 11, and 15). Although the Proterozoic grains in Tamaulipas beach sand may have been supplied from Grenville basement sources along the Colorado River in central Texas (e.g., Blum et al., 2017),

a southward increase along the Tamaulipas coastline in combined Yavapai-Mazatzal grains (1800–1500 Ma) and Granite-Rhyolite grains (1500–1320 Ma) is difficult to explain by such a phenomenon. A second observation is that Late Cretaceous grains, common in the river sediment of Nuevo León and Tamaulipas yet absent from our Rio Grande samples, are consistently present in Tamaulipas beach sand (Figs. 8, 11, and 15). Because dams in northeastern Mexico currently intercept sediment in the rivers that drain to the lower Rio Grande, we infer that the Late Cretaceous zircon grains in Tamaulipas beaches are being reworked from coastal plain sediment deposited prior to the construction of the dams. Similarly, the comparative scarcity of late Paleozoic and Triassic grains in Tamaulipas beaches is attributed to impoundment of Sierra Madre Oriental–sourced sand in reservoirs.

Southward transport of sand along Mexico's eastern coast indicates that winter surface currents on the shelf dominate the littoral transport system (Fig. 15). Nevertheless, the ultimate fate of sand that moves south along the western Gulf of Mexico beaches remains uncertain. There are no obvious submarine canyons in southern Veracruz delivering sediment across the shelf to deep water, although strong evidence exists for a Miocene submarine canyon that crossed the marine shelf near the mouth of the Río Papaloapan (Fig. 2) and funneled a large volume of sediment to the Veracruz Fan in the deepest reaches of the Gulf of Mexico (Hessler et al., 2018).

CONCLUSIONS

Modern beach sands along the coastline of the western Gulf of Mexico vary systematically in composition from north to south. Beaches of Tamaulipas contain significant percentages of quartz not predicted by the predominantly carbonate source rocks in the Sierra Madre Oriental of northeastern Mexico and abundant detrital zircon grain ages that indicate ultimate sediment sources in the southern Rocky Mountains of the United States. Detectable proportions of sediment having Rocky Mountain provenance persist in Mexican beach sand as far south as central Veracruz, more than 3600 km from the Rocky Mountain region where Paleoproterozoic basement rocks are exposed. The observed trends in sediment composition indicate long-term, south-directed sediment transport in the littoral zone. The Rio Grande currently supplies some of the coastal sediment, but beach sands of Tamaulipas contain more abundant Proterozoic (1.8–1.5 Ga, 1.5–1.32 Ga, and 1.1 Ga) grains from the Rocky Mountain region and more Jurassic and Late Cretaceous grains previously transported by rivers from the adjacent Sierra Madre Oriental,

but currently impounded in reservoirs in northeastern Mexico, than does Rio Grande sediment. This suggests that littoral transport in the western Gulf of Mexico recycles coastal plain sediment of northeastern Mexico that was deposited prior to the construction of dams in the Rio Grande catchment.

Progressive southward enrichment in volcanic lithic grains and Neogene to Quaternary detrital zircon ages in Mexican beach sand indicate increased influence of sediment derived from volcanic sources in Mexico and likewise corroborate net south-directed littoral transport. Although sedimentary lithic grains dominate sediment of some rivers draining the Sierra Madre Oriental, volcanic lithic grain proportions are most abundant in sediment of river catchments that tap the southeastern extent of the Paleogene Sierra Madre Occidental volcanic field and the active Trans-Mexican volcanic belt of central Mexico. The silicic composition and vast extent of the Sierra Madre Occidental volcanic field and correlative volcanic fields in northern Mexico and the southwestern United States cause Eocene–Oligocene zircon grains to dominate most modern sands of eastern Mexico. Nevertheless, modern rivers and beaches of Veracruz contain abundant mafic to intermediate volcanic grains and zircon grains having Miocene to recent ages (20–0 Ma). These volcanic grains and young zircons were derived from the Trans-Mexican volcanic belt.

Compositional variations of sediment in the coastal zone provide a useful complement to oceanographic data, which may provide an ambiguous view of potential net sediment transport. Future studies of modern sand composition will provide important input to quantitative models of coastal sand budget at the sea-land interface, a critical sector to human economies and coastal ecosystems.

and geology, which served as a template for Figure 2, and we are grateful to Lucy Tingwei Ko (Bureau of Economic Geology) for assistance with the photomicrographs. We also thank Julian Clark (Equinor) and members of the Statoil Research Center in Austin for informative discussions regarding Mexican sediment routing. Reviews by Eduardo Garzanti and Theresa Schwartz greatly improved the text and data presentation. We thank associate editor Emily Finzel for editorial supervision.

REFERENCES CITED

Alemán-Gallardo, E.A., Ramírez-Fernández, J.A., Rodríguez-Díaz, A.A., Velasco-Tapia, F., Jenchen, U., Cruz-Gámaz, E.M., De León-Barragán, L., and Navarro-De León, I., 2019, Evidence for an Ordovician continental arc in the pre-Mesozoic basement of the Huizachal-Peregrina anticlinorium, Sierra Madre Oriental, Mexico: Peregrina Tonalite: Mineralogy and Petrology, v. 113, p. 505–525, https://doi.org/10.1007/s00710-019-00660-4.

Anderson, T.H., and Silver, L.T., 2005, The Mojave-Sonora megashear—Field and analytical studies leading to the conception and evolution of the hypothesis, *in* Anderson, T.H., Nourse, J.A., McKee, J.W., and Steiner, M.B., eds., The Mojave-Sonora Megashear Hypothesis: Development, Assessment, and Alternatives: Geological Society of America Special Paper 393, p. 1–50, https://doi.org/10.1130/0-8137-2393-0.1.

Barboza-Gudiño, J.R., Zavala-Monsiváis, A., Venegas-Rodríguez, G., and Barajas-Nigoche, L.D., 2010, Late Triassic stratigraphy and facies from northeastern Mexico: Tectonic setting and provenance: Geosphere, v. 6, p. 621–640, https://doi.org/10.1130/GES00545.1.

Bascomb, W., 1980, Waves and Beaches: The Dynamics of the Ocean Surface: Garden City, New York, Anchor Press/Doubleday, 366 p.

Blum, M.D., Milliken, K.T., Pecha, M.A., Snedden, J.W., Frederick, B.C., and Galloway, W.E., 2017, Detrital-zircon records of Cenomanian, Paleocene, and Oligocene Gulf of Mexico drainage integration and sediment routing: Implications for scales of basin-floor fans: Geosphere, v. 13, p. 2169–2205, https://doi.org/10.1130/GES01410.1.

Bryan, S.E., Ferrari, L., Reiners, P.W., Allen, C.M., Petrone, C.M., Ramos-Rosique, A., and Campbell, I.H., 2008, New insights into crustal contributions to large-volume rhyolite generation in the mid-Tertiary Sierra Madre Occidental province, Mexico, revealed by U-Pb geochronology: Journal of Petrology, v. 49, p. 47–77, https://doi.org/10.1093/petrology/egm070.

Cardona, A., Chew, D., Valencia, V.A., Bayona, G., Mišković, A., and Ibañez-Mejía, M., 2010, Grenvillian remnants in the northern Andes: Rodinian and Phanerozoic paleogeographic perspectives: Journal of South American Earth Sciences, v. 29, p. 92–104, https://doi.org/10.1016/j.jsames.2009.07.011.

Cepeda, J.C., and Henry, C.D., 1983, Oligocene Volcanism and Multiple Caldera Formation in the Chinati Mountains, Presidio County, Texas: Austin, Texas, Bureau of Economic Geology Report of Investigations 135, 32 p.

Chako Tchambé, B., Carrasco-Núñez, G., Miggins, D.P., and Németh, K., 2020, Late Pleistocene to Holocene activity of Alchichica maar volcano, eastern Trans-Mexican volcanic belt: Journal of South American Earth Sciences, v. 97, https://doi.org/10.1016/j.jsames.2019.102404.

Chapin, C.E., 2012, Origin of the Colorado mineral belt: Geosphere, v. 8, p. 28–43, https://doi.org/10.1130/GES00694.1.

Corfu, F., Hanchar, J.M., Hoskin, P.W.O., and Kinny, P., 2003, Atlas of zircon textures, *in* Hanchar, J.M., and Hoskin, P.W.O., eds., Zircon: Reviews in Mineralogy & Geochemistry, v. 53, p. 469–502, https://doi.org/10.1515/9781501509322-019.

Critelli, S., and Ingersoll, R.V., 1995, Interpretation of neovolcanic versus palaeovolcanic sand grains: An example from Miocene deep-marine sandstone of the Topanga Group (southern California): Sedimentology,

v. 42, p. 783–804, https://doi.org/10.1111/j.1365-3091.1995.tb00409.x.

Díaz-Bravo, B.A., Barboza-Gudiño, J.R., Ortega-Obregón, C., and Morales-Gámez, M., 2022, Late Cretaceous to Oligocene overlapping plutonic magmatism episodes in the eastern Mesa Central province of Mexico: International Geology Review, v. 64, p. 675–697, https://doi.org/10.1080/00206814.2021.1871866.

Dickinson, W.R., 1985, Interpreting provenance from detrital modes of sandstones, *in* Zuffa, G.G., ed., Provenance of Arenites: Dordrecht, Netherlands, D. Reidel, p. 333–361, https://doi.org/10.1007/978-94-017-2809-6_15.

Dickinson, W.R., and Gehrels, G.E., 2003, U-Pb ages of detrital zircons from Permian and Jurassic eolian sandstones of the Colorado Plateau, USA: Paleogeographic implications: Sedimentary Geology, v. 163, p. 29–66, https://doi.org/10.1016/S0037-0738(03)00158-1.

Dickinson, W.R., and Gehrels, G.E., 2009a, U-Pb ages of detrital zircons in Jurassic eolian and associated sandstones of the Colorado Plateau: Evidence for transcontinental dispersal and intraregional recycling of sediment: Geological Society of America Bulletin, v. 121, p. 408–433, https://doi.org/10.1130/B26406.1.

Dickinson, W.R., and Gehrels, G.E., 2009b, Use of U-Pb ages of detrital zircons to infer maximum depositional ages of strata: A test against a Colorado Plateau Mesozoic database: Earth and Planetary Science Letters, v. 288, p. 115–125, https://doi.org/10.1016/j.epsl.2009.09.013.

Dickinson, W.R., and Lawton, T.F., 2001, Carboniferous to Cretaceous assembly and fragmentation of Mexico: Geological Society of America Bulletin, v. 113, p. 1142–1160, https://doi.org/10.1130/0016-7606(2001)113<1142:CTCAAF>2.0.CO;2.

Dickinson, W.R., Beard, L.S., Brakenridge, G.R., Erjavec, J.K., Ferguson, R.C., Inman, K.F., Knepp, R.A., Lindberg, F.A., and Ryberg, P.T., 1983, Provenance of North American Phanerozoic sandstones in relation to tectonic setting: Geological Society of America Bulletin, v. 94, p. 222–235, https://doi.org/10.1130/0016-7606(1983)94<222:PONAPS>2.0.CO;2.

Dickinson, W.R., Lawton, T.F., and Gehrels, G.E., 2009, Recycling detrital zircons: A case study from the Cretaceous Bisbee Group of southern Arizona: Geology, v. 37, p. 503–506, https://doi.org/10.1130/G25646A.1.

Fan, M., Brown, E., and Li, L., 2019, Cenozoic drainage evolution of the Rio Grande paleoriver recorded in detrital zircons in south Texas: International Geology Review, v. 61, p. 622–636, https://doi.org/10.1080/00206814.2018.1446368.

Ferrari, L., López-Martínez, M., and Rosas-Elguera, J., 2002, Ignimbrite flare-up and deformation in the southern Sierra Madre Occidental, western Mexico: Implications for the late subduction history of the Farallon plate: Tectonics, v. 21, https://doi.org/10.1029/2001TC001302.

Ferrari, L., Valencia-Moreno, M., and Bryan, S., 2005, Magmatismo y tectónica en la Sierra Madre Occidental y su relación con la evolución de la margen occidental de Norteamerica: Boletín de la Asociación Geológica Mexicana, v. 57, p. 343–378, https://doi.org/10.18268/BSGM2005v57n3a5.

Ferrari, L., Valencia-Moreno, M., and Bryan, S., 2007, Magmatism and tectonics of the Sierra Madre Occidental and its relation with the evolution of the western margin of North America, *in* Alaniz-Álvarez, S.A., and Nieto-Samaniego, A.F., eds., Geology of México: Celebrating the Centenary of the Geological Society of México: Geological Society of America Special Paper 422, p. 1–39, https://doi.org/10.1130/2007.2422(01).

Ferrari, L., Orozco-Esquivel, M., Manea, V., and Manea, M., 2012, The dynamic history of the Trans-Mexican volcanic belt and the Mexico subduction zone: Tectonophysics, v. 522–523, p. 122–149, https://doi.org/10.1016/j.tecto.2011.09.018.

Fitz-Díaz, E., Lawton, T.F., Juárez-Arriaga, E., and Chávez-Cabello, G., 2018, The Cretaceous–Paleogene Mexican orogen: Structure, basin development, magmatism and tectonics: Earth-Science Reviews, v. 183, p. 56–84, https://doi.org/10.1016/j.earscirev.2017.03.002.

Garzanti, E., 2016, From static to dynamic provenance analysis—Sedimentary petrology upgraded: Sedimen-

tary Geology, v. 336, p. 3–13, https://doi.org/10.1016/j.sedgeo.2015.07.010.

Garzanti, E., Andò, S., Vezzoli, G., Lustrino, M., Boni, M., and Vermeesch, P., 2012, Petrology of the Namib Sand Sea: Long-distance transport and compositional variability in the wind-displaced Orange Delta: Earth-Science Reviews, v. 112, p. 173–189, https://doi.org/10.1016/j.earscirev.2012.02.008.

Garzanti, E., Vermeesch, P., Al-Ramadan, K.A., Andò, S., Limonta, M., Rittner, M., and Vezzoli, G., 2017, Tracing transcontinental sand transport: From Anatolia–Zagros to the Rub' Al Khali Sand Sea: Journal of Sedimentary Research, v. 87, p. 1196–1213, https://doi.org/10.2110/jsr.2017.65.

Gehrels, G.E., Blakey, R., Karlstrom, K.E., Timmons, J.M., Dickinson, B., and Pecha, M., 2011, Detrital zircon U-Pb geochronology of Paleozoic strata in the Grand Canyon, Arizona: Lithosphere, v. 3, p. 183–200, https://doi.org/10.1130/L121.1.

Giles, K.D., Jackson, W.T., Jr., McKay, M.P., Beebe, D.A., Larsen, D., Kwon, Y., and Shaulis, B., 2023, Sediment input, alongshore transport, and coastal mixing in the northeastern Gulf of Mexico based on detrital-zircon geochronology: Marine and Petroleum Geology, v. 148, https://doi.org/10.1016/j.marpetgeo.2022.105997.

Goff, F., and Gardner, J.N., 2004, Late Cenozoic geochronology of volcanism and mineralization in the Jemez Mountains and Valles caldera, north central New Mexico, *in* Mack, G.H., and Giles, K.A., eds., The Geology of New Mexico: A Geologic History: New Mexico Geological Society Special Publication 11, p. 295–312.

Gómez-Alvarez, F., Garduño-Monroy, V.H., Sosa-Ceballos, G., Jiménez-Haro, A., Liotta, D., Gaitan-Ramirez, M.F., Brogi, A., Israde-Alcántara, I., Majera-Blas, S.M., Wheeler, W., Forster, M., and Garcia-Hernández, O.H., 2021, New constraints on tectonism and magmatism from the eastern sector of the Trans-Mexican volcanic belt (Chignahuapan horst, Puebla, México): Journal of South American Earth Sciences, v. 112, https://doi.org/10.1016/j.jsames.2021.103468.

Gómez-Tuena, A., Cavazos-Tovar, J.G., Parolari, M., Straub, S.M., and Espinasa-Pereña, R., 2018, Geochronological and geochemical evidence of continental crust 'relamination' in the origin of intermediate arc magmas: Lithos, v. 322, p. 52–66, https://doi.org/10.1016/j.lithos.2018.10.005.

Gray, G.G., Pottorf, R.J., Yurewicz, D.A., Mahon, K.I., Pevear, D.R., and Chuchla, R.J., 2001, Thermal and chronological record of syn- to post-Laramide burial and exhumation, Sierra Madre Oriental, Mexico, *in* Bartolini, C., Buffler, R.T., and Cantu Chapa, A., eds., The Western Gulf of Mexico Basin: Tectonics, Sedimentary Basins, and Petroleum Systems: American Association of Petroleum Geologists Memoir 75, p. 159–181, https://doi.org/10.1306/M75768C7.

Gray, G.G., Villagomez, D., Pindell, J., Molina-Garza, R.S., O'Sullivan, P., Stockli, D., Farrel, W., Blank, D., and Schuba, J., 2020, Late Mesozoic and Cenozoic thermotectonic history of eastern, central and southern Mexico as determined through integrated thermochronology, with implications for sediment delivery to the Gulf of Mexico, *in* Davison, I., Hull, J.N.F., and Pindell, J., eds., The Basins, Orogens and Evolution of the Southern Gulf of Mexico and Northern Caribbean: Geological Society, London, Special Publication 504, p. 255–283, https://doi.org/10.1144/SP504-2019-243.

Hessler, A.M., Covault, J.A., Stockli, D.F., and Fildani, A., 2018, Late Cenozoic cooling favored glacial over tectonic controls on sediment supply to the western Gulf of Mexico: Geology, v. 46, p. 995–998, https://doi.org/10.1130/G45528.1.

Hoskin, P.W.O., and Schaltegger, U., 2003, The composition of zircon and igneous and metamorphic petrogenesis, *in* Hanchar, J.M., and Hoskin, P.W.O., eds., Zircon: Reviews in Mineralogy & Geochemistry, v. 53, p. 27–62, https://doi.org/10.1515/9781501509322-005.

Hudec, M.R., Dooley, T.P., Peel, F.J., and Soto, J.I., 2020, Controls on the evolution of passive-margin salt basins: Structure and evolution of the Salina del Bravo region, northeastern Mexico: Geological Society of America Bulletin, v. 132, p. 997–1012, https://doi.org/10.1130/B35283.1.

Hudson, P.F., 2003, Event sequence and sediment exhaustion in the lower Panuco basin, Mexico: Catena, v. 52, p. 57–76, https://doi.org/10.1016/S0341-8162(02)00145-5.

Ingersoll, R.V., and Suczek, C.A., 1979, Petrology and provenance of Neogene sand from Nicobar and Bengal fans, DSDP sites 211 and 218: Journal of Sedimentary Petrology, v. 49, p. 1217–1228, https://doi.org/10.1306/212F78F1-2B24-11D7-8648000102C1865D.

Ingersoll, R.V., Bullard, T.F., Ford, R.L., Grimm, J.P., Pickle, J.D., and Sares, S.W., 1984, The effect of grain size on detrital modes: A test of the Gazzi-Dickinson point-counting method: Journal of Sedimentary Petrology, v. 54, p. 103–116, https://doi.org/10.1306/212F83B9-2B24-11D7-8648000102C1865D.

Ingersoll, R.V., Cavazza, W., Graham, S.A., and I.U.G.F.S. Participants, 1987, Provenance of impure calclithites in the Laramide foreland of southwestern Montana: Journal of Sedimentary Petrology, v. 57, p. 995–1003, https://doi.org/10.1306/212F8CC9-2B24-11D7-8648000102C1865D.

Iriondo, A., Premo, W.R., Martínez-Torres, L.M., Budahn, J.R., Atkinson, W.W., Jr., Siems, D.F., and Guarás-Gonzáles, B., 2004, Isotopic, geochemical, and temporal characterization of Proterozoic basement rocks in the Quitovac region, northwestern Sonora, Mexico: Implications for the reconstruction of the southwestern margin of Laurentia: Geological Society of America Bulletin, v. 116, p. 154–170, https://doi.org/10.1130/B25138.1.

Jackson, S.E., Pearson, N.J., Griffin, W.L., and Belousova, E.A., 2004, The application of laser ablation–inductively coupled plasma–mass spectrometry to in situ U-Pb zircon geochronology: Chemical Geology, v. 211, p. 47–69, https://doi.org/10.1016/j.chemgeo.2004.06.017.

Juárez-Arriaga, E., Lawton, T.F., Ocampo-Díaz, Y.Z.E., Stockli, D.F., and Solari, L., 2019a, Sediment provenance, sediment-dispersal systems, and major arc-magmatic events recorded in the Mexican foreland basin, north-central and northeastern Mexico: International Geology Review, v. 61, p. 2118–2142, https://doi.org/10.1080/00206814.2019.1581848.

Juárez-Arriaga, E., Lawton, T.F., Stockli, D.F., Solari, L., and Martens, U., 2019b, Late Cretaceous–Paleocene stratigraphic and structural evolution of the central Mexican fold and thrust belt, from detrital zircon (U-Th)/(He-Pb) ages: Journal of South American Earth Sciences, v. 95, https://doi.org/10.1016/j.jsames.2019.102264.

LaMaskin, T.A., 2012, Detrital zircon facies of Cordilleran terranes in western North America: GSA Today, v. 22, no. 3, p. 4–11, https://doi.org/10.1130/GSATG142A.1.

Lawlor, P.J., Ortega-Gutierrez, F., Cameron, K.L., Ochoa-Camarillo, H., Lopez, R., and Sampson, D.E., 1999, U-Pb geochronology, geochemistry, and provenance of the Grenvillian Huiznopala Gneiss of eastern Mexico: Precambrian Research, v. 94, p. 73–99, https://doi.org/10.1016/S0301-9268(98)00108-9.

Lawton, T.F., Bradford, I.A., Vega, F.J., Gehrels, G.E., and Amato, J.M., 2009, Provenance of Upper Cretaceous–Paleogene sandstones in the foreland basin system of the Sierra Madre Oriental, northeastern Mexico, and its bearing on fluvial dispersal systems of the Mexican Laramide Province: Geological Society of America Bulletin, v. 121, p. 820–836, https://doi.org/10.1130/B26450.1.

Lawton, T.F., Hunt, G.J., and Gehrels, G.E., 2010, Detrital zircon record of thrust belt unroofing in Lower Cretaceous synorogenic conglomerates, central Utah: Geology, v. 38, p. 463–466, https://doi.org/10.1130/G30684.1.

Leary, R.J., Umhoefer, P., Smith, M.E., Smith, T.M., Saylor, J.E., Riggs, N., Burr, G., Lodes, E., Foley, D., Licht, A., Mueller, M.A., and Baird, C., 2020, Provenance of Pennsylvanian–Permian sedimentary rocks associated with the Ancestral Rocky Mountains orogeny in southwestern Laurentia: Implications for continental-scale Laurentian sediment transport systems: Lithosphere, v. 12, p. 88–121, https://doi.org/10.1130/L1115.1.

Lipman, P.W., and McIntosh, W.C., 2008, Eruptive and non-eruptive calderas, northeastern San Juan Mountains, Colorado: Where did ignimbrites come from?: Geological Society of America Bulletin, v. 120, p. 771–795, https://doi.org/10.1130/B26330.1.

Liu, L., Stockli, D.F., Lawton, T.F., Xu, J., Stockli, L.D., Fan, M., and Nadon, G.C., 2022, Reconstructing source-to-sink systems from detrital zircon core and rim ages: Geology, v. 50, p. 691–696, https://doi.org/10.1130/G49904.1.

Ludwig, K.R., 2003, Isoplot 3.00: Berkeley Geochronology Center Special Publication 4, 70 p.

Mack, G.H., McIntosh, W.C., Leeder, M.R., and Monger, H.C., 1996, Plio-Pleistocene pumice floods in the ancestral Rio Grande, southern Rio Grande rift, USA: Sedimentary Geology, v. 103, p. 1–8, https://doi.org/10.1016/0037-0738(96)00009-7.

Marsaglia, K.M., 1991, Provenance of sands and sandstones from a rifted continental arc, Gulf of California, Mexico, *in* Fisher, R.V., and Smith, G.A., eds., Sedimentation in Volcanic Settings: Society for Sedimentary Geology (SEPM) Special Publication 45, p. 237–248, https://doi.org/10.2110/pec.91.45.0237.

Marsaglia, K.M., and Ingersoll, R.V., 1992, Compositional trends in arc-related, deep-marine sand and sandstone: A reassessment of magmatic-arc provenance: Geological Society of America Bulletin, v. 104, p. 1637–1649, https://doi.org/10.1130/0016-7606(1992)104<1637:CTIARD>2.3.CO;2.

Marsh, J.H., and Stockli, D.F., 2015, Zircon U-Pb and trace element zoning characteristics in an anatectic granulite domain: Insights from LASS-ICP-MS depth profiling: Lithos, v. 239, p. 170–185, https://doi.org/10.1016/j.lithos.2015.10.017.

Martin, A.J., Domènech, M., Stockli, D.F., and Gómez-Gras, D., 2022, Provenance and maximum depositional ages of Upper Triassic and Jurassic sandstone, north-eastern Mexico: Basin Research, v. 34, p. 1164–1190, https://doi.org/10.1111/bre.12654.

McIntosh, W.C., Chapin, C.E., Ratté, J.C., and Sutter, J.F., 1992, Time-stratigraphic framework for the Eocene-Oligocene Mogollon-Datil volcanic field, southwest New Mexico: Geological Society of America Bulletin, v. 104, p. 851–871, https://doi.org/10.1130/0016-7606(1992)104<0851:TSFFTE>2.3.CO;2.

Milliman, J.D., and Farnsworth, K.L., 2011, River Discharge to the Coastal Ocean: A Global Synthesis: Cambridge, UK, Cambridge University Press, 384 p., https://doi.org/10.1017/CBO9780511781247.

Molina Garza, R.S., Lawton, T.F., Barboza Gudiño, J.R., Sierra-Rojas, M.I., Guadarrama, A.F., and Pindell, J., 2020, Geochronology and correlation of the Todos Santos Group, western Veracruz and eastern Oaxaca States, Mexico: Implications for regional stratigraphic relations and the rift history of the Gulf of Mexico, *in* Martens, U., and Molina Garza, R.S., eds., Southern and Central Mexico: Basement Framework, Tectonic Evolution, and Provenance of Mesozoic–Cenozoic Basins: Geological Society of America Special Paper 546, p. 143–170, https://doi.org/10.1130/2020.2546(06).

Moore, S., Heise, E.A., Grove, M., Reisinger, A., and Benavides, J.A., 2021, Evaluating the impacts of dam construction and longshore transport upon modern sedimentation within the Rio Grande delta (Texas, U.S.A.): Journal of Coastal Research, v. 37, p. 26–40, https://doi.org/10.2112/JCOASTRES-D-20-00049.1.

Nasholds, M.W.M., and Zimmerer, M.J., 2022, High-precision ⁴⁰Ar/³⁹Ar geochronology and volumetric investigation of volcanism and resurgence following eruption of the Tshirege Member, Bandelier Tuff, at the Valles caldera: Journal of Volcanology and Geothermal Research, v. 431, https://doi.org/10.1016/j.jvolgeores.2022.107624.

Ortega-Flores, B., Solari, L.A., Lawton, T.F., and Ortega-Obregón, C., 2014, Detrital zircon record of major Middle Triassic–Early Cretaceous provenance shift, central Mexico: Demise of Gondwanan continental fluvial systems and onset of backarc volcanism and sedimentation: International Geology Review, v. 56, p. 237–261, https://doi.org/10.1080/00206814.2013.844313.

Ortega-Gutiérrez, F., Elías-Herrera, M., Morán-Zenteno, D.J., Solari, L., Luna-González, L., and Schaaf, P., 2014, A review of batholiths and other plutonic intrusions of Mexico: Gondwana Research, v. 26, p. 834–868, https://doi.org/10.1016/j.gr.2014.05.002.

Ramos-Vázquez, M.A., and Armstrong-Altrin, J.S., 2021, Provenance of sediments from Barra del Tordo and Tesoro beaches, Tamaulipas State, northwestern Gulf of Mexico: Journal of Palaeogeography, v. 10, 20, https://doi.org/10.1186/s42501-021-00101-4.

Rosales-Lagarde, L., Centeno-García, E., Dostal, J., Sour-Tovar, F., Ochoa-Camarillo, H., and Quiroz-Barroso, S., 2005, The Tuzancoa Formation: Evidence of an early Permian submarine continental arc in east-central Mexico: International Geology Review, v. 47, p. 901–919, https://doi.org/10.2747/0020-6814.47.9.901.

Ross, C.H., Stockli, D.F., Rasmussen, C., Gulick, S.P.S., de Graaff, S.J., Claeys, P., Zhao, J., Xiao, L., Pickersgill, A.E., Schmieder, M., Kring, D.A., Wittmann, A., and Morgan, J.V., 2022, Evidence of Carboniferous arc magmatism preserved in the Chicxulub impact structure: Geological Society of America Bulletin, v. 134, p. 241–260, https://doi.org/10.1130/B35831.1.

Rubio-Cisneros, I.I., and Lawton, T.F., 2011, Detrital zircon U-Pb ages of sandstones in continental red beds at Valle de Huizachal, Tamaulipas, NE Mexico: Record of Early–Middle Jurassic arc volcanism and transition to crustal extension: Geosphere, v. 7, p. 159–170, https://doi.org/10.1130/GES00567.1.

Saylor, J.E., and Sundell, K.E., 2016, Quantifying comparison of large detrital geochronology data sets: Geosphere, v. 12, p. 203–220, https://doi.org/10.1130/GES01237.1.

Self, R.P., 1975, Petrologic changes in fluvial sediments in the Rio Nautla drainage basin, Veracruz, Mexico: Journal of Sedimentary Petrology, v. 45, p. 140–149, https://doi.org/10.1306/212F6CEE-2B24-11D7-8648000102C1865D.

Self, R.P., 1977, Longshore variation in beach sands, Nautla area, Veracruz, Mexico: Journal of Sedimentary Petrology, v. 47, p. 1437–1443, https://doi.org/10.1306/212F7388-2B24-11D7-8648000102C1865D.

Sharman, G.R., and Malkowski, M.A., 2020, Needles in a haystack: Detrital zircon U-Pb ages and the maximum depositional age of modern global sediment: Earth-Science Reviews, v. 203, https://doi.org/10.1016/j.earscirev.2020.103109.

Sharman, G.R., Sharman, J.P., and Sylvester, Z., 2018, detritalPy: A Python-based toolset for visualizing and analysing detrital geo-thermochronologic data: The Depositional Record: The Journal of Biological, Physical and Geochemical Sedimentary Processes, v. 4, p. 202–215, https://doi.org/10.1002/dep2.45.

Sláma, J., Kosler, J., Condon, D.J., Crowley, J.L., Gerdes, A., Hanchar, J.M., Horstwood, M.S.A., Morris, G.A., Nasdala, L., Norberg, N., Schaltegger, U., Schoene, B., Tubrett, M.N., and Whitehouse, M.J., 2008, Plešovice zircon—A new natural reference material for U-Pb and Hf isotopic microanalysis: Chemical Geology, v. 249, p. 1–35, https://doi.org/10.1016/j.chemgeo.2007.11.005.

Smye, A.J., and Stockli, D.F., 2014, Rutile U-Pb age depth profiling: A continuous record of lithospheric thermal evolution: Earth and Planetary Science Letters, v. 408, p. 171–182, https://doi.org/10.1016/j.epsl.2014.10.013.

Spell, T.L., McDougall, I., and Doulgeris, A.P., 1996, Cerro Toledo Rhyolite, Jemez volcanic field, New Mexico: ⁴⁰Ar/³⁹Ar geochronology of eruptions between two caldera-forming events: Geological Society of America Bulletin, v. 108, p. 1549–1566, https://doi.org/10.1130/0016-7606(1996)108<1549:CTRJVF>2.3.CO;2.

Suter, M., 1990, Hoja Tamazunchale 14Q-e (5): Con Geología de la Hoja Tamazunchale, Estados de Hidalgo, Querétaro y San Luis Potosí: México, D.F., Instituto de Geología, Universidad Nacional Autónoma de México (1 sheet), scale 1:100,000.

Thomson, K.D., Stockli, D.F., and Fildani, A., 2022, Anthropogenic impact on sediment transfer in the upper Missouri River catchment detected by detrital zircon analysis: Geological Society of America Bulletin, v. 134, p. 2485–2502, https://doi.org/10.1130/B36217.1.

Van Andel, T.H., and Poole, D.M., 1960, Sources of recent sediments in the northern Gulf of Mexico: Journal of Sedimentary Petrology, v. 30, p. 91–122, https://doi.org/10.1306/74D709D4-2B21-11D7-8648000102C1865D.

van de Kamp, P.C., 2018, Provenance and alteration of feldspathic and quartzose sediments in southern Mexico: An application of Krynine's hypothesis on second-cycle arkose, *in* Ingersoll, R.V., Lawton, T.F., and Graham, S.A., eds., Tectonics, Sedimentary Basins, and Provenance: A Celebration of William R. Dickinson's Career: Geological Society of America Special Paper 549, p. 89–117, https://doi.org/10.1130/2018.2540(05).

Van der Plas, L., and Tobi, A.C., 1965, A chart for judging the reliability of point counting results: American Journal of Science, v. 263, p. 87–90, https://doi.org/10.2475/ajs.263.1.87.

Velasco-Tapia, F., Martínez-Paco, M., Iriondo, A., Ocampo-Díaz, Y.Z.E., Cruz-Gámez, E.M., Ramos-Ledezma, A., Andaverde, J.A., Ostrooumov, M., and Masuch, D., 2016, Altered volcanic ash layers of the Late Cretaceous San Felipe Formation, Sierra Madre Oriental (northeastern Mexico): U-Pb geochronology, provenance and tectonic setting: Journal of South American Earth Sciences, v. 70, p. 18–35, https://doi.org/10.1016/j.jsames.2016.04.010.

Vermeesch, P., 2004, How many grains are needed for a provenance study?: Earth and Planetary Science Letters, v. 224, p. 441–451, https://doi.org/10.1016/j.epsl.2004.05.037.

Vermeesch, P., 2013, Multi-sample comparison of detrital age distributions: Chemical Geology, v. 341, p. 140–146, https://doi.org/10.1016/j.chemgeo.2013.01.010.

Whitmeyer, S.J., and Karlstrom, K.E., 2007, Tectonic model for the Proterozoic growth of North America: Geosphere, v. 3, p. 220–259, https://doi.org/10.1130/GES00055.1.

Zavala-Hidalgo, J., Morey, S.L., and O'Brien, J.J., 2003, Seasonal circulation on the western shelf of the Gulf of Mexico using a high-resolution numerical model: Journal of Geophysical Research, v. 108, no. C12, https://doi.org/10.1029/2003JC001879.